7-26-2018

A Numerical Investigation of Multiple Traveling Pulse and Front Solutions

Faisal Duraihem
University of Connecticut - Storrs, faisal.duraihem@uconn.edu

A Numerical Investigation of Multiple Traveling Pulse and Front Solutions

Faisal Duraihem, Ph.D.

University of Connecticut, 2018

ABSTRACT

Algorithms are proposed to calculate traveling pulses and fronts in both directions for the FitzHugh- Nagumo equations in one dimensional spatial domain. The first algorithm is based on the application of the steepest descent method to a certain functional on some admissible sets. These sets are different for pulses and for fronts. This approach is global in nature, so that an initial guess for the wave profile and the speed can be quite different from the correct solution. The second algorithm is the pseudo arc length continuation method, which solves the governing equations directly. The two algorithms are complementary. Continuation makes the computation of a bifurcation diagram more efficient, but it requires a good initial guess. This is supplied by the steepest descent algorithm. Also, the two algorithms serve as an independent check for one another.

Depending on the physical parameter values, we observe the existence of single, multiple (stable and unstable) or no traveling pulses and fronts, within the corresponding admissible set. At suitable parameter values, we found as many as five traveling wave solutions; two distinct pulses and two fronts moving to the right, and one front moving to the left. The computed wave profiles are tested numerically using

a parabolic solver and, for stable solutions, the speed and shape are maintained very well for a large number of time steps.

A Numerical Investigation of Multiple Traveling Pulse and Front Solutions

Faisal Duraihem

M.S. University of Connecticut, 2016

B.S. King Saud University, 2000

A Dissertation

Submitted in Partial Fulfillment of the

Requirements for the Degree of

Doctor of Philosophy

at the

University of Connecticut

2018

APPROVAL PAGE

Doctor of Philosophy Dissertation

A Numerical Investigation of Multiple Traveling Pulse and Front Solutions

Presented by

Faisal Duraihem, B.S. Math., M.S. Math.

Major Advisor _____
Yung Choi

Major Advisor _____
Jeffrey Connors

Associate Advisor _____
Dmitriy Leykekhman

University of Connecticut

2018

ACKNOWLEDGMENTS

First and foremost, I would like to thank God Almighty for giving me the strength, knowledge, ability and opportunity to undertake this research study and to persevere and complete it satisfactorily. Without his blessings, this achievement would not have been possible.

Special thanks should be given to Dr. Yung Choi, my research project supervisor for his professional guidance and valuable support and to Dr. Jeffrey Connors for his useful and constructive recommendations on this research work. Their willingness to give their time, enthusiastic encouragement and useful critiques generously has been very much appreciated. My grateful thanks are also extended to my mother and family for their support and encouragement throughout my study.

Finally, my thanks go to all the people who have supported me to complete the research work directly or indirectly.

Contents

Ch. 1. A steepest descent method 1

1.1 Introduction 1

1.2 A variational formulation for traveling waves 4

1.2.1 Case 1: Pulses 6

1.2.2 Case 2: Fronts 7

1.3 A steepest descent method for the computation of traveling waves . . 8

1.3.1 Case 1: Pulses 8

1.3.2 Case 2: Fronts 12

1.4 Fronts traveling in both directions 12

Ch. 2. Numerical implementation and boundary conditions 14

2.1 Numerical implementation of the steepest descent algorithm 14

2.2 Asymptotic boundary conditions for $\mathcal{L}_c u$ 16

2.3 Asymptotic boundary conditions for u^* 19

Ch. 3. Continuation algorithm 21

3.1 The governing equations for a continuation algorithm 21

3.2 Continuation 24

3.2.1 Before engaging the continuation algorithm 25

3.2.2 The continuation algorithm 27

3.2.3 Pseudo arc length continuation 27

3.3 Asymptotic boundary conditions 29

3.3.1 At $x = \infty$ (for both pulse and front) 29

3.3.2 At $x = -\infty$ for the pulse 31

3.3.3 At $x = -\infty$ for the front 32

3.4 Discretization of the governing equations 33

Ch. 4. Numerical results 35
4.1 Numerical results of the steepest descent algorithm 35
4.1.1 Case 1: Pulses 36
4.1.2 Case 2: Front moving to the right 41
4.1.3 Case 3: Front moving to the left 46
4.1.4 An independent check of our algorithm 50
4.2 Numerical results for the continuation algorithm 51
4.2.1 Solution dependence on d 51
4.2.2 Solution dependence on γ 53

Chapter 1

A steepest descent method

1.1 Introduction

Reaction-diffusion models are commonly studied in diverse phenomena in physics, chemistry and biology [12]. For infinite domains their equilibrium solutions are known as standing waves. Besides being important in their own right, these are crucial in understanding the dynamics of time-evolving solutions, as the latter may approach the standing waves as time evolves. These stable standing waves are then known as local attractors (of time-evolving trajectories). Traveling waves are another special solution to reaction-diffusion systems. To an observer moving with a certain speed c, these kinds of solutions appear stationary and keep their own shape. In fact, a standing wave corresponds to $c = 0$. These solutions can be local attractors as well [8]. A determination of a traveling wave involves both its shape and wave speed.

Since the first important traveling wave paper [9] in the 1930's, traveling wave solutions of scalar second order reaction-diffusion equations have been studied exten-

sively [11]. However progress has been slow on a system of equations, unless the maximum principles happen to be applicable [10]. FitzHugh-Nagumo equations are not in the latter category. Recently there are known theoretical results for the equations. With the help of this new information, we would like to numerically demonstrate the richness of phenomena associated with this system. We will construct global numerical algorithms for computing traveling waves and show that multiple traveling wave solutions can coexist with the same physical parameters.

Let $d > 0$, $\gamma > 0$, $0 < \beta < 1/2$ be given parameters satisfying

$$\frac{4}{(1-\beta)^2} < \gamma < \frac{9}{(1-2\beta)(2-\beta)} \tag{1.1.1}$$

and let $f(u) \equiv u(u-\beta)(1-u)$. The FitzHugh-Nagumo equations are given by

$$\begin{cases} u_t = u_{xx} + \frac{1}{d}(f(u) - v) \quad , \\ v_t = v_{xx} + u - \gamma\, v \quad . \end{cases} \tag{1.1.2}$$

The imposed bounds on γ in (1.1.1) will be explained later on in this subsection. We look for their traveling wave solutions. In other words, do there exist bounded smooth functions $\tilde{u} : \mathbb{R} \to \mathbb{R}$, $\tilde{v} : \mathbb{R} \to \mathbb{R}$ and a constant $c \in \mathbb{R}$ such that $u(x,t) = \tilde{u}(x-ct)$ and $v(x,t) = \tilde{v}(x-ct)$ are solutions of (1.1.2)? This requires

$$\begin{cases} \tilde{u}'' + c\tilde{u}' + \frac{1}{d}(f(\tilde{u}) - \tilde{v}) = 0, \\ \tilde{v}'' + c\tilde{v}' + \tilde{u} - \gamma\tilde{v} = 0. \end{cases} \tag{1.1.3}$$

If $c > 0$ then the wave travels to the right. After a rescaling of the independent

variable, the governing traveling wave equations are

$$c^2 du'' + c^2 du' + f(u) - v = 0, \tag{1.1.4a}$$

$$c^2 v'' + c^2 v' + u - \gamma v = 0. \tag{1.1.4b}$$

Constant equilibrium solutions of (1.1.4a) and (1.1.4b) satisfy

$$\begin{cases} f(u) - v = 0, \\ u - \gamma v = 0. \end{cases} \tag{1.1.5}$$

When $\gamma > \frac{4}{(1-\beta)^2}$ as specified in (1.1.1), there are three equilibrium states $(u, v) = (0, 0), (\mu_2, \frac{\mu_2}{\gamma}), (\mu_3, \frac{\mu_3}{\gamma})$ with $0 < \beta < \mu_2 < \frac{1+\beta}{2} < \mu_3 < 1$. Multiple equilibrium states can lead to two types of traveling wave solutions: a front and a pulse. A traveling front solution connects distinct equilibrium states at both ends while a traveling pulse connects the same equilibrium state. We will look for both traveling pulse and traveling front solutions with $(u, v) \to (0, 0)$ as $x \to \infty$ while their behavior as $x \to -\infty$ differ.

Before we focus our attention on the FitzHugh-Nagumo equations, we examine the case of a scalar parabolic equation $w_t = w_{xx} + f(w)$ with the same bistable nonlinearity f as above. Its constant equilibrium solutions are $w = 0$, β, 1. Suppose $w(x, t) = u(x - ct) \equiv u(\zeta)$ is its traveling wave solution with a speed $c > 0$, then the waves travels to the right and $u'' + cu' + f(u) = 0$. Moreover u goes to a constant equilibrium solution as $\zeta \to \pm\infty$. Define $T(u) \equiv \frac{u'^2}{2} - F(u)$ where $F(u) = -\int_0^u f(t)dt$.

A direct computation gives

$$\frac{dT}{d\zeta} = u'\left(u'' + f(u)\right) = -cu'^2 \leq 0.$$

For a non-trivial u, it is clear that

$$T(u(\infty)) = -F(u(\infty)) < T(u(-\infty)) = -F(u(-\infty)),$$

hence there will never be a traveling pulse; only a front satisfying $F(u(\infty)) > F(u(-\infty))$ is possible. With $\beta < \frac{1}{2}$ it can be checked that $F(\beta) > 0 = F(0) > F(1)$. Suppose $u = 0$ at $x = \infty$, it follows that only $u = 1$ at $x = -\infty$ is a feasible choice. If we think of F as the energy, when the wave travels to the right, eventually the lower energy state $u = 1$ will displace the higher energy state $u = 0$.

We like to numerically investigate if analogous statements can be made for the FitzHugh-Nagumo equations. The corresponding theoretical study has been conducted in [6].

1.2 A variational formulation for traveling waves

Recall from [2] the following variational formulation for the solutions of (1.1.4a) and (1.1.4b); the formulation works for both pulses and fronts. Define the Hilbert spaces $L^2_{e^x} \equiv \{u : \int e^x w^2 dx < \infty\}$ with the inner product $\langle f, g\rangle_{L^2_{e^x}} = \int e^x fg\, dx$, and $H^1_{e^x} \equiv \{u : \int e^x(u'^2 + u^2)dx < \infty\}$ with the inner product $\langle f, g\rangle_{H^1_{e^x}} = \int e^x(f'g' + fg)\, dx$. As (1.2.4b) is a linear equation in v we can let $v \equiv \mathcal{L}_c u$. Here the linear operator

$\mathcal{L}_c : L^2_{e^x} \to L^2_{e^x}$ is defined by

$$\mathcal{L}_c u(x) \equiv \int_{-\infty}^{\infty} G(x,s)u(s)ds,$$

where $G(x,s)$ is the Green's function

$$G(x,s) = \begin{cases} \frac{1}{c\sqrt{c^2+4\gamma}} \mathrm{e}^{r_2(x-s)} & if \quad x < s, \\ \frac{1}{c\sqrt{c^2+4\gamma}} \mathrm{e}^{r_1(x-s)} & if \quad x > s, \end{cases}$$

with $r_1 = \frac{-c-\sqrt{c^2+4\gamma}}{2c} < -1$ and $r_2 = \frac{-c+\sqrt{c^2+4\gamma}}{2c} > 0$. Define $F : \mathbb{R} \to \mathbb{R}$ by $F(\xi) \equiv -\int_0^\xi f(\eta)d\eta = \frac{\xi^4}{4} - \frac{(1+\beta)\xi^3}{3} + \frac{\beta\xi^2}{2}$ and $J_c : H^1_{e^x} \to \mathbb{R}$ by

$$J_c(u) \equiv \int_{\mathbb{R}} e^x \left(\frac{dc^2}{2} u_x^2 + \frac{1}{2} u\mathcal{L}_c u + F(u) \right) dx. \tag{1.2.1}$$

As $\mathcal{L}_c$ is self-adjoint with respect to the weighted inner product in $L^2_{e^x}$, i.e. for any $f, g \in L^2_{e^x}$, $\langle f, \mathcal{L}_c g \rangle_{L^2_{e^x}} = \langle \mathcal{L}_c f, g \rangle_{L^2_{e^x}}$, a direct calculation gives

$$J_c'(u)h = \int_{\mathbb{R}} e^x \left(dc^2 u_x h_x + h\mathcal{L}_c u - f(u)h \right) dx \quad \text{for all } h \in \ H^1_{e^x}. \tag{1.2.2}$$

Hence unconstrained critical points of J_c satisfy the integral differential equation

$$c^2 du'' + c^2 du' + f(u) - \mathcal{L}_c u = 0,$$

which is equivalent to (1.1.4a)-(1.1.4b).

1.2.1 Case 1: Pulses

Following [2] we employ a definition which will be used in the admissible domain $\mathcal{A}_p$ for studying pulses below.

Definition: A function $u \in C(\mathbb{R})$ is in the class $-/+/-$ if there exist $x_1, x_2 \in [-\infty, \infty]$ with $x_1 \leq x_2$ such that (a) $u(x) \leq 0$ for all $x \in (-\infty, x_1] \cup [x_2, \infty)$ and (b) $u(x) \geq 0$ for all $x \in [x_1, x_2]$.

Take a constant $M_1 = M_1(\gamma) > 0$ such that for all $\xi \leq -M_1$, we have $f(\xi) \geq \frac{1}{\gamma}$. Let

$$\mathcal{A}_p \equiv \{u \in H^1_{e^x} : \|u\|^2_{H^1_{e^x}} = 2, -M_1 \leq u \leq 1, u \in -/+/-\}.$$

We look for a minimizer u_0 of J_c restricted to the domain $\mathcal{A}_p$. Introduce a Lagrange multiplier λ to remove the equality constraint $\|u\|^2_{H^1_{e^x}} = 2$ in $\mathcal{A}_p$. It follows that u_0 is an unconstrained critical point of $\mathcal{I}_c$ where

$$\mathcal{I}_c(u) \equiv J_c(u) + \lambda \left(\int_{\mathbb{R}} e^x \frac{1}{2}(u'^2 + u^2) dx - 1 \right). \tag{1.2.3}$$

Hence for all $\phi \in H^1_{e^x}$

$$0 = \mathcal{I}'_c(u_0)\phi = J'_c(u_0)\phi + \lambda \int_{\mathbb{R}} e^x (u'_0\phi' + u_0\phi) dx. \tag{1.2.4}$$

Putting $\phi = u'_0$ this becomes

$$0 = \int_{\mathbb{R}} e^x \left(dc^2 \left(\frac{u'^2_0}{2} \right)' + \left(\frac{u_0 \mathcal{L}_c u_0}{2} \right)' + (F(u_0))' \right) dx + \lambda \int_{\mathbb{R}} \frac{e^x}{2} \left(u'^2_0 + u^2_0 \right)' dx.$$

An integration by parts yields $J_c(u_0) + \lambda = 0$. If we can pick $c = c_0$ such that

$J_{c_0}(u_0) = 0$, then $\lambda = 0$. This allows us to conclude from (1.2.4) and (1.2.2) that u_0 and $v_0 = \mathcal{L}_{c_0}(u_0)$ solve (1.1.4a) and (1.1.4b). In other words (u_0, v_0, c_0) is a traveling wave solution. While this argument has ignored the inequality constraints in $\mathcal{A}_p$, the same conclusion can be drawn by the rigorous proof in [2].

1.2.2 Case 2: Fronts

In order to have a traveling front solution, we need more then one constant equilibrium solution; hence $\gamma > \frac{4}{(1-\beta)^2}$ is imposed. Recall that $(u, v) = (0, 0), (\mu_2, \frac{\mu_2}{\gamma}), (\mu_3, \frac{\mu_3}{\gamma})$ are the constant equilibrium solutions.

We now explain the physical significance of the other condition $\gamma < \frac{9}{(1-2\beta)(2-\beta)}$ in (1.1.1). Let $E = \frac{1}{2}u\mathcal{L}_c u + F(u)$ be the energy, which includes the nonlocal energy as well. (This is motivated by the form of J_c in (1.2.1). Note that $u_x = 0$ for a constant equilibrium solution). The equilibrium solution $(u, v) = (0, 0)$ has an energy of $E_1 = 0$; while that for $(u, v) = (\mu_3, \frac{\mu_3}{\gamma})$ is $E_3 = \frac{\mu_3^2}{2\gamma} + F(\mu_3)$. When $\gamma = \gamma^* = \frac{9}{(1-2\beta)(2-\beta)}$, let $\mu_3 = \mu_3^*$. It can be checked that

$$\int_0^{\mu_3^*} \left(\frac{u}{\gamma} - f(u) \right) du = 0;$$

i.e. the areas of the two regions formed by the straight line $v = \frac{u}{\gamma^*}$ and $v = f(u)$ are equal and opposite in signs. Suppose $\gamma < \gamma^*$ as in (1.2.1), then

$$E_1 = 0 < \int_0^{\mu_3} \left(\frac{u}{\gamma} - f(u) \right) du = \frac{\mu_3^2}{2\gamma} + F(\mu_3) = E_3. \tag{1.2.5}$$

At the end of Section 1.1, we have demonstrated that only a lower energy state can displace a higher energy state for traveling waves of a scalar parabolic equation. We

will investigate if the same will be true for a traveling front of the FitzHugh-Nagumo equations. See [5].

Definition: A function $u \in C(\mathbb{R})$ is in the class $+/-$ if there exist $x_1 \in [-\infty, \infty]$ such that (a) $u(x) \geq 0$ for all $x \in (-\infty, x_1]$ and (b) $u(x) \leq 0$ for all $x \in [x_1, \infty)$.

To study traveling fronts we let

$$\mathcal{A}_f \equiv \{u \in H^1_{e^x} : \|u\|^2_{H^1_{e^x}} = 2, -M_1 \leq u \leq 1, u \in +/- \text{ and } u - \mu_3 \in +/-\}.$$

Note that $+/- \subseteq -/+/-$ as we allow x_1 and x_2 in the defintion of $-/+/-$ to take up $\pm\infty$.

We look for a minimizer u_f of J_c in the domain $\mathcal{A}_f$. Similar arguments as in the case of a pulse lead to finding a speed c_f such that $J_{c_f}(u_f) = 0$. Then (u_f, v_f, c_f) is a traveling front solution where $v_f = \mathcal{L}_{c_f} u_f$ with $(u_f, v_f) \to (\mu_3, \frac{\mu_3}{\gamma})$ as $x \to -\infty$ and $(u_f, v_f) \to (0, 0)$ as $x \to \infty$. If $c_f > 0$, the higher energy state $(\mu_3, \frac{\mu_3}{\gamma})$ will displace the lower energy state $(0, 0)$. On the other hand if $c_f < 0$, the lower energy state $(0, 0)$ displaces the higher energy state $(\mu_3, \frac{\mu_3}{\gamma})$.

1.3 A steepest descent method for the computation of traveling waves

1.3.1 Case 1: Pulses

We propose to find (u_0, v_0, c_0) numerically using a steepest descent algorithm, which tracks a global minimizer u_0 of J_c in the admissible set $\mathcal{A}_p$. Pioneering work has already been done in [5]. Given any $c > 0$ and $u \in \mathcal{A}_p$, let the steepest descent direction

on the manifold $\{u \in H^1_{e^x} : \|u\|^2_{H^1_{e^x}} = 2\}$ be denoted by $q = q(u, c)$, normalized so that $\|q\|^2_{H^1_{e^x}} = 2$. It can now be checked that $\langle u, q\rangle_{H^1_{e^x}} = 0$. We introduce Lagrange multipliers ρ and μ to remove the equality constraints $\|q\|^2_{H^1_{e^x}} = 2$ and $\langle u, q\rangle_{H^1_{e^x}} = 0$, respectively. Therefore q can be found as an unconstrained critical point of

$$\mathcal{K}_c(\phi) = J'_c(u)\phi + \rho(\frac{1}{2}\|\phi\|^2_{H^1_{e^x}} - 1) + \mu\langle u, \phi\rangle_{H^1_{e^x}} \quad \text{for all } \phi \in H^1_{e^x}. \tag{1.3.1}$$

Hence we have

$$\mathcal{K}'_c(q) = 0 \tag{1.3.2}$$

with

$$\mathcal{K}'_c(\phi)p = J'_c(u)p + \rho\langle \phi, p\rangle_{H^1_{e^x}} + \mu\langle u, p\rangle_{H^1_{e^x}} \quad \text{for all } p \in H^1_{e^x}. \tag{1.3.3}$$

From (1.3.2) and (1.3.3) we have

$$0 = J'_c(u)p + \rho\langle q, p\rangle_{H^1_{e^x}} + \mu\langle u, p\rangle_{H^1_{e^x}} \quad \text{for all } p \in H^1_{e^x}. \tag{1.3.4}$$

Putting $p = u$ in (1.3.4) we get

$$J'_c(u)u + \rho\langle q, u\rangle_{H^1_{e^x}} + \mu\|u\|^2_{H^1_{e^x}} = 0. \tag{1.3.5}$$

As $\|u\|^2_{H^1_{e^x}} = 2$ and $\langle q, u\rangle_{H^1_{e^x}} = 0$, we get $\mu = \frac{-1}{2}J'_c(u)u$, which is computable. Returning to (1.3.4) we have for all $p \in H^1_{e^x}$,

$$\begin{aligned}\int_{\mathbb{R}} e^x \left(dc^2u'p' + p\mathcal{L}_c u - f(u)p\right) dx + \rho\int_{\mathbb{R}} e^x(q'p' + qp)dx \\ + \mu\int_{\mathbb{R}} e^x(u'p' + up)dx = 0,\end{aligned} \tag{1.3.6}$$

which implies

$$-u^*_{xx} - u^*_x + u^* = dc^2 u - \mathcal{L}_c u + f(u), \tag{1.3.7}$$

where $u^* = \rho q + (dc^2 + \mu)u$. For a pulse we impose $|u^*(x)| \to 0$ as $x \to \infty$.

Observe that (1.3.7) is a linear equation. Given $c > 0$ and an approximation $u = u^n \in H^1_{e^x}$ for a minimizer of J_c, the right hand side of (1.3.7) is known and we can numerically solve u^* using the finite difference method [1, 6]. (See details in Chapter 2). As a consequence we can compute ρq. It can be shown ρq points in the steepest descent direction. Hence the next update is

$$u^{n+1} = u^n + \alpha(u^* - (\mu + dc^2)u^n), \quad 0 < \alpha < 1. \tag{1.3.8}$$

Here α is the descent step size, which is chosen by us through experimentation. When $J_c(u^n)$ stops decreasing, we have found a minimizer numerically. Thus we have a minimizer $u_0^{(c)}$ such that $J_c(u_0^{(c)}) = \inf_{\mathcal{A}_p} J_c \equiv \mathcal{J}(c)$. These procedures allow us to obtain a graph of $\mathcal{J}$ versus c. It is known [2] that there is always a $c = c_0$ such that $\mathcal{J}(c) \equiv J_c(u_0^{(c)}) = 0$ when d is sufficiently small. Let $v_0^{(c_0)} = \mathcal{L}_{c_0} u_0^{(c_0)}$. Then $(u_0^{(c_0)}, v_0^{(c_0)}, c_0)$ is a traveling pulse solution.

Algorithm. Given $c > 0$and $u^n \in \mathcal{A}_p$, the steepest descent algorithm to compute $\min_{\mathcal{A}_p} J_c$ is as follows

1- Compute $v^n = \mathcal{L}_c u^n$.

2- Set $\mu^n = -\frac{1}{2} J_c'(u^n) u^n$.

3- Compute u^*, for $u = u^n$ in (1.3.7).

4- Set $\tilde{u}^{n+1} = u^n + \alpha(u^* - (\mu + dc^2)u^n)$.

5- Set $u^{n+1} = s(r(\tilde{u}^{n+1}))$, where r is the clipping operator, and s is the shift operator

(see below).

6- Check $J(u^{n+1}) \leq J(u^n)$.

Here the clipping and the shift operators are defined as follows.

Definition. Let

$$u \in C_0^+ \equiv \{u \in C(\mathbb{R}) : u(x) > 0 \text{ for some } x \in \mathbb{R} \text{ and } \lim_{|x|\to\infty} u(x) = 0\}$$

be given and define

$$\bar{x} \equiv \max\{x \in \mathbb{R} : u(x) = \max_{y\in\mathbb{R}} u(y)\}.$$

Let (x_1, x_2) be the largest open interval containing $\bar{x}$ such that $u(x) > 0$ for all $x \in (x_1, x_2)$. We define the clipping operator $r : C_0^+ \to -/+/-$ such that for any $u \in C_0^+$

$$r(u)(x) = \begin{cases} u(x), & if \quad x \in (x_1, x_2) \text{ or } u(x) \leq 0, \\ 0, & \text{otherwise.} \end{cases}$$

Definition. The shift operator $s : H^1_{e^x} \to H^1_{e^x}$ is defined such that for any $u \in H^1_{e^x}$,

$$s(u)(x) = u(x - \log\frac{1}{\omega}),$$

where $\omega = \frac{1}{2}\|u\|^2_{H^1_{e^x}}$.

Step 5 in the above algorithm ensures that $u^{n+1} \in -/+/-$ and $\|u^{n+1}\|^2_{H^1_{e^x}} = 2$. In fact we should also clip in case $u^{n+1} < -M_1$; however in all our computations we have never observed this happening.

1.3.2 Case 2: Fronts

The traveling front satisfies $(u, v) \to (0, 0)$ as $x \to \infty$ and $(u, v) \to (\mu_3, \frac{\mu_3}{\gamma})$ as $x \to -\infty$. Hence its right boundary condition will be the same as that for a pulse, while there is a difference at the left boundary. In actual numerical implementation the domain $(-\infty, \infty)$ will be approximated by a long interval $[a, b]$. We will discuss how to construct asymptotic boundary conditions at both $x = a$ and $x = b$ in the next chapter. It turns out that so long as $u' \to 0$ (which is satisfied by both pulse and front), the asymptotic boundary conditions remains the same. Since $u \in +/-$ and $u - \mu \in +/-$ for a front, there will be a difference for the clipping operation in step 5 of the algorithm. As the change is more or less obvious, we skip the details.

1.4 Fronts traveling in both directions

Let a front satisfy $(u, v) \to (0, 0)$ as $x \to \infty$ and $(u, v) \to (\mu_3, \frac{\mu_3}{\gamma})$ as $x \to -\infty$. For γ in the range specified by (1.1.1), we know from (1.2.5) that $E_1 < E_3$. For a traveling front with $c > 0$, the high energy equilibrium state will displace the low energy state; this is exactly opposite the scalar equation situation. Our numerical results in Chapter 4 show indeed there is such a solution.

On the other hand, it seems likely that a low energy state can also displace a high energy state. If such a solution also exists, we have a second front solution which travels to the left. In order to use the same algorithm to find this second front solution, we make the following transformation.

Our traveling front problem is to find (u, v, c) satisfying

$$\begin{cases} dc^2u'' + dc^2u' + f(u) - v = 0, \\ c^2v'' + c^2v' + u - \gamma v = 0, \end{cases} \tag{1.4.1}$$

with $(u, v) \to (\mu_3, \frac{\mu_3}{\gamma})$ as $x \to -\infty$ and $(u, v) \to (0, 0)$ as $x \to \infty$. To look for a front traveling to the left, let $U = \mu_3 - u$ and $V = \frac{\mu_3}{\gamma} - v$. Thus we have

$$\begin{cases} -dc^2U'' - dc^2U' + f(\mu_3 - U) - \frac{\mu_3}{\gamma} + V = 0, \\ -c^2V'' - c^2V' + \mu_3 - U - \gamma(\frac{\mu_3}{\gamma} - V) = 0. \end{cases} \tag{1.4.2}$$

which are the same as

$$\begin{cases} dc^2U'' + dc^2U' + \tilde{f}(U) - V = 0, \\ c^2V'' + c^2V' - \gamma V + U = 0, \end{cases} \tag{1.4.3}$$

where $\tilde{f}(U) = \frac{\mu_3}{\gamma} - f(\mu_3 - U)$. Observe that $(U, V) \to (0, 0)$ as $x \to \infty$ and $(U, V) \to (\mu_3, \frac{\mu_3}{\gamma})$ as $x \to -\infty$. In Chapter 4 we are able to use our existing steepest decent algorithm to find a right traveling front $(U, V, \tilde{c})$ with speed $\tilde{c} > 0$. Going back to the original variables (u, v), this new traveling front correspond to a wave traveling to the left. The state $(u, v) = (0, 0)$ will eventually displace $(u, v) = (\mu_3, \frac{\mu_3}{\gamma})$, resulting in a lower energy state displacing a higher energy state.

Chapter 2

Numerical implementation and boundary conditions

2.1 Numerical implementation of the steepest descent algorithm

In the first step of our steepest descent algorithm in Section 1.3.1, for a given $c > 0$ we need to compute $v = \mathcal{L}_c u$, i.e. v satisfies the linear equation

$$-c^2 v_{xx} - c^2\, v_x - \ u + \gamma\, v = 0. \tag{2.1.1}$$

Approximate $(-\infty, \infty)$ by a large interval $[a, b]$ and take a uniform mesh $\{x_0, x_1, ..., x_N\}$ with $x_0 = a$, $x_N = b$, and $x_j - x_{j-1} = h = \frac{b-a}{N}$ for $j = 1, 2, ..., N$. To solve this equation we use a centered, second-order finite difference method and obtain

$$(-v_{j+1} + 2v_j - v_{j-1}) - \tfrac{h}{2}(v_{j+1} - v_{j-1}) + h^2 \tfrac{\gamma}{c^2} v_j = \tfrac{h^2}{c^2} u_j, \quad j = 0, 1, 2, ..., N, \tag{2.1.2}$$

with asymptotic boundary conditions at the end points to be described in the next section.

Second, we compute $\mu = \frac{-1}{2} J_c'(u)u$ by applying a composite midpoint quadrature rule

$$\mu = -\frac{h}{2} \sum_{j=0}^{N} e^{x_{j+1/2}} \{ dc^2 \left(\tfrac{u_{j+1}-u_j}{h} \right)^2 + u_{j+1/2} v_{j+1/2} - f(u_{j+1/2}) u_{j+1/2} \}, \tag{2.1.3}$$

where $u_{j+1/2} = \frac{u_j + u_{j+1}}{2}$ and $v_{j+1/2} = \frac{v_j + v_{j+1}}{2}$.

Third, u^* can be solved by using a similar finite difference discretization on (1.3.7) with corresponding asymptotic boundary conditions. This allows evaluation of $\tilde{u}^{n+1}$ and u^{n+1} in steps 4 and 5 of the steepest descent algorithm. In particular, after we perform the clipping operation, the shifting operation can now be easily achieved by updating the node locations :

$$x_j^{n+1} = x_j^n + \log \left(\frac{2}{\|r(\tilde{u}^{n+1})\|^2_{H^1_{ex}}} \right), \quad j = 0, 1, ..., N. \tag{2.1.4}$$

Next, we compute

$$J_c(u^{n+1}) = h \sum_{j=0}^{N} e^{x^n_{j+1/2}} \left\{ \frac{dc^2}{2} \left(\frac{u^n_{j+1} - u^n_j}{h} \right)^2 + \frac{1}{2} u^n_{j+1/2} v^n_{j+1/2} + F(u^n_{j+1/2}) \right\} \tag{2.1.5}$$

where v^{n+1} is solved from u^{n+1} using an analogue of (2.1.2), $u^{n+1}_{j+1/2} = \frac{1}{2}(u^{n+1}_j + u^{n+1}_{j+1})$ and $v^{n+1}_{j+1/2} = \frac{1}{2}(v^{n+1}_j + v^{n+1}_{j+1})$.

Finally we check if $J_c(u^{(n+1)}) \leq J_c(u^{(n)})$. The algorithm stops when

$$\frac{J_c(u^{(n)}) - J_c(u^{(n+1)})}{J_c(u^{(n+1)})} \leq \delta_1$$

or

$$J_c(u^{(n)}) - J_c(u^{(n+1)}) \leq \delta_2$$

for some prescribed small δ_1 and δ_2. We take $\delta_2 \ll \delta_1$ in our implementation. The second condition is needed when $J_c \approx 0$.

2.2 Asymptotic boundary conditions for $\mathcal{L}_c u$

We now construct asymptotic boundary conditions for (2.1.1). Suppose a function $u \in C(\mathbb{R})$ is known only on a large interval $[a, b]$. Let $v = \mathcal{L}_c u$ so that

$$v'' + v' - \frac{\gamma}{c^2} v = -\frac{u}{c^2} \tag{2.2.1}$$

on $(-\infty, \infty)$. This is equivalent to the system:

$$\begin{pmatrix} v \\ z \end{pmatrix}' = A \begin{pmatrix} v \\ z \end{pmatrix} - \begin{pmatrix} 0 \\ \frac{u}{c^2} \end{pmatrix} \tag{2.2.2}$$

where $A = \begin{pmatrix} 0 & 1 \\ \frac{\gamma}{c^2} & -1 \end{pmatrix}$. The eigenvalues of A are $\lambda_{1,2} = \frac{1}{2}\left(-1 \pm \sqrt{1 + \frac{4\gamma}{c^2}}\right)$ with $\lambda_1 < -1 < 0 < \lambda_2$ and the corresponding left eigenvectors are $\vec{\ell}_1 = \begin{pmatrix} -\lambda_2 \\ 1 \end{pmatrix}$ and

$\vec{\ell}_2 = \begin{pmatrix} -\lambda_1 \\ 1 \end{pmatrix}$. By taking the scalar product of $\vec{\ell}_1$ with (2.2.2), we obtain

$$\varphi_1' = \lambda_1 \varphi_1 - \frac{u}{c^2}, \tag{2.2.3}$$

where $\varphi_1 \equiv \vec{\ell}_1 . \begin{pmatrix} v \\ z \end{pmatrix} = -\lambda_2 v + z$. This first order equation can be cast in the form

$$(e^{-\lambda_1 t}\varphi_1)' = -\frac{u}{c^2} e^{-\lambda_1 t}.$$

As we restrict our attention to bounded u and v, φ_1 has to be bounded. Hence

$$e^{-\lambda_1 x}\varphi_1(x) = -\int_{-\infty}^{x} \frac{u(t)}{c^2} e^{-\lambda_1 t} dt,$$

which simplifies to

$$\varphi_1(x) = -\int_{-\infty}^{x} \frac{u(t)}{c^2} e^{\lambda_1 (x-t)} dt.$$

In other words, the arbitrary constant associated with the complementary solution of (25) has to be set to zero in order for φ_1 to stay bounded as $x \to -\infty$. With $(-\infty, \infty)$ being approximated by the large interval $[a, b]$ for the purpose of numerical computation and u being known only on $[a, b]$, we now estimate $\varphi_1(a)$. First we observe

$$-\frac{u(a)}{c^2} = \lambda_1 \int_{-\infty}^{a} e^{\lambda_1 (a-t)} \frac{u(a)}{c^2} dt.$$

Thus

$$\lambda_1 \varphi_1(a) - \frac{u(a)}{c^2} = \frac{\lambda_1}{c^2} \int_{-\infty}^{a} e^{\lambda_1 (a-t)} (u(a) - u(t)) dt$$

$$= \frac{-1}{c^2} \int_{-\infty}^{a} e^{\lambda_1(a-t)} u'(t) dt.$$

For both traveling fronts and pulses, we can assume $u'(t) = o(1)$ as $t \to -\infty$. Thus if $|a| \gg 1$ and $a < 0$, then

$$|\lambda_1 \varphi_1(a) - \frac{u(a)}{c^2}| \leq \frac{|o(1)|}{c^2} \int_{-\infty}^{a} e^{\lambda_1(a-t)} dt = \frac{|o(1)|}{|\lambda_1| c^2}.$$

We therefore employ the asymptotic boundary condition $\lambda_1 \varphi_1 = \frac{u}{c^2}$ at $x = a$. This is equivalent to

$$v' - \lambda_2 v = \frac{u}{\lambda_1 c^2} \quad \text{at } x = a. \tag{2.2.4}$$

A similar analysis leads to

$$v' - \lambda_1 v = \frac{u}{\lambda_2 c^2} \quad \text{at } x = b. \tag{2.2.5}$$

The asymptotic boundary conditions are (2.2.4) and (2.2.5).

Recall that $x = a$ corresponds to the mesh point x_0. Setting $j = 0$ in (2.1.2) we have

$$-v_1 + 2v_0 - v_{-1} - \frac{h}{2}(v_1 - v_{-1}) + h^2 \frac{\gamma}{c^2} v_0 = \frac{h^2}{c^2} u_0. \tag{2.2.6}$$

On the other hand, a discretization of (2.2.4) gives

$$v_1 - v_{-1} - 2h\lambda_2 v_0 = \frac{2h}{\lambda_1 c^2} u_0. \tag{2.2.7}$$

After some algebraic manipulation to eliminate v_{-1}, we obtain

$$(2 + 2h\lambda_2 + \frac{h^2\gamma}{c^2} - h^2\lambda_2) v_0 - 2v_1 = \frac{h^2}{c^2} \left(1 + \frac{1}{\lambda_1} - \frac{2}{h\lambda_1}\right) u_0. \tag{2.2.8}$$

An analogous derivation gives

$$(2 - 2h\lambda_1 + \frac{h^2\gamma}{c^2} - h^2\lambda_1)v_N - 2v_{N-1} = \frac{h^2}{c^2}\left(1 + \frac{1}{\lambda_2} + \frac{2}{h\lambda_2}\right)u_N \tag{2.2.9}$$

at the right boundary $x = b$, which corresponds to the mesh point x_N.

We note that the discretized boundary conditions (2.2.8) and (2.2.9) work for both the pulse and front solutions.

2.3 Asymptotic boundary conditions for u^*

We will compute u^* from (1.3.7). Let $\tilde{u} = dc^2u - \mathcal{L}_c u + f(u)$, which is known. Hence we study

$$u^{*\prime\prime} + u^{*\prime} - u^* = \tilde{u}.$$

Comparing this equation to (2.1.1), the asymptotic boundary condition analysis in Section 2.2 are applicable if we substitute γ/c^2 by 1 and u/c^2 by $\tilde{u}$. Hence the new eigenvalues are

$$\lambda^*_{1,2} = \frac{1}{2}\left(-1 \pm \sqrt{5}\right)$$

while the asymptotic boundary conditions are given by

$$u^{*\prime} - \lambda^*_2 u^* = \frac{\tilde{u}}{\lambda^*_1} \quad \text{at } x = a. \tag{2.3.1}$$

$$u^{*\prime} - \lambda^*_1 u^* = \frac{\tilde{u}}{\lambda^*_2} \quad \text{at } x = b. \tag{2.3.2}$$

The new discretized asymptotic boundary conditions are then

$$\left(2 + 2h\lambda_2^* + h^2 - h^2\lambda_2^*\right) u_0^* - 2u_1^* = h^2 \left(1 + \frac{1}{\lambda_1^*} - \frac{2}{h\lambda_1^*}\right) \tilde{u}_0 \tag{2.3.3}$$

and

$$(2 - 2h\lambda_1^* + h^2 - h^2\lambda_1^*)u_N^* - 2u_{N-1}^* = h^2 \left(1 + \frac{1}{\lambda_2^*} + \frac{2}{h\lambda_2^*}\right) \tilde{u}_N \tag{2.3.4}$$

where $\tilde{u_j} = dc^2 u_j - v_j + f(u_j)$.

Chapter 3

Continuation algorithm

3.1 The governing equations for a continuation algorithm

The steepest descent algorithm that we develop for both traveling pulses and fronts are global in nature. There is no need for a good initial guess in order for the algorithm to converge. Once we have found one such solution using the algorithm, a continuation method can be used in conjunction to find other solutions when the physical parameters are changed gradually. This can lead to a more efficient numerical method and allow us to trace the solution curves in a bifurcation diagram.

The traveling wave problem is to find (u_0, v_0, c_0) satisfying (1.1.4a) and (1.1.4b). Since any translation of a solution remains a solution, we impose a constraint

$$\int_{-\infty}^{\infty} e^x(u'^2 + u^2)dx = 2$$

to make the solution unique. Otherwise, there will be a non-trivial null space to the linearized operator which will cause a breakdown of the continuation method. In addition we want to pick c_0 so that $J_{c_0}(u_0, v_0) = 0$.

First we demonstrate that this last equation is satisfied automatically if (1.1.4a) and (1.1.4b) hold. Indeed suppose (u, v, c) satisfies (1.1.4a) and (1.1.4b). Define

$$J_c(u) \equiv \int_{\mathbb{R}} e^x \left(\frac{dc^2}{2} u'^2 + \frac{1}{2} u \mathcal{L}_c u + F(u) \right) dx.$$

Then for any $\phi \in H^1_{e^x}(\mathbb{R})$,

$$\begin{aligned} J_c'(u)\phi &= \int_{\mathbb{R}} e^x \left(dc^2 u'\phi' + \phi \mathcal{L}_c u - f(u)\phi \right) dx && (3.1.1) \\ &= \int_{\mathbb{R}} e^x \left(-dc^2 u'' - dc^2 u' + \mathcal{L}_c u - f(u) \right) \phi dx && (3.1.2) \\ &= 0 && (3.1.3) \end{aligned}$$

because of (1.1.4a)-(1.1.4b). In particular, if we take $\phi = u'$ in (3.1.1),

$$\begin{aligned} 0 &= J_c'(u)u' \\ &= \int_{\mathbb{R}} e^x \left(dc^2 u'u'' + u'\mathcal{L}_c u - f(u)u' \right) dx \\ &= \int_{\mathbb{R}} e^x \frac{d}{dx} \left(\frac{dc^2}{2} u'^2 + \frac{1}{2} u \mathcal{L}_c u + F(u) \right) dx \\ &= -\int_{\mathbb{R}} e^x \left(\frac{dc^2}{2} u'^2 + \frac{1}{2} u \mathcal{L}_c u + F(u) \right) dx \\ &= -J_c(u), \end{aligned}$$

where the last equality has been obtained using integration by parts. Thus $J_c(u) = 0$ is automatic. We can therefore conclude that in a numerical implementation of

a continuation algorithm for the FitzHugh-Nagumo equations, there is no need to enforce $J_c(u) = 0$. It suffices to find (u, v, c) satisfying

$$c^2 du'' + c^2 du' + f(u) - v = 0, \tag{3.1.4a}$$

$$c^2 v'' + c^2 v' + u - \gamma v = 0, \tag{3.1.4b}$$

$$\int_{-\infty}^{\infty} e^x (u'^2 + u^2) dx - 2 = 0. \tag{3.1.4c}$$

These are the governing equations for the continuation algorithm.

Define $g : C^2(\mathbb{R}) \times C^2(\mathbb{R}) \times \mathbb{R} \times \mathbb{R}^3 \to C(\mathbb{R}) \times C(\mathbb{R}) \times \mathbb{R}$ such that for $u, v \in C^2(\mathbb{R}), c \in \mathbb{R}$ and $\vec{p} = (d, \gamma, \beta) \in \mathbb{R}^3$,

$$g(u, v, c, \vec{p}) \equiv \begin{pmatrix} c^2 du'' + c^2 du' + f(u) - v \\ c^2 v'' + c^2 v' + u - \gamma v \\ \int_{-\infty}^{\infty} e^x (u'^2 + u^2) dx - 2 \end{pmatrix}. \tag{3.1.5}$$

As a reminder, β is embedded in the definition of the function f. Traveling waves are the solutions that satisfy $g(u, v, c, \vec{p}) = 0$ when parameter $\vec{p}$ is given. Finding a solution is difficult because the system of equations are nonlinear. However for a given set of physical parameters d, γ, β, our global steepest descent algorithm already finds solutions without a good initial guess. Once we have one solution point, we can find other solutions using a continuation algorithm. In actual implementation, we fix two of (d, γ, β) and call the third λ. A continuation algorithm computes the solution curve as we vary λ gradually.

3.2 Continuation

We now describe the continuation method [9]. For our specific application to the equations (3.1.4a)-(3.1.4c), we can think of $X = C^2(\mathbb{R}) \times C^2(\mathbb{R}) \times \mathbb{R}$, $Y = C(\mathbb{R}) \times C(\mathbb{R}) \times \mathbb{R}$, $\lambda \in \mathbb{R}$ is one of $\{d, \gamma, \beta\}$ while the other two parameters are fixed, and $x = (u, v, c) \in X$.

Let X, Y be Banach spaces and $g : X \times \mathbb{R} \to Y$ be C^1. We like to find (x, λ) so that $g(x, \lambda) = 0$. As $g \in C^1$, for any $(x, \lambda) \in X \times \mathbb{R}$ we have the partial derivative $D_x g(x, \lambda) \in \mathcal{L}(X, Y)$, the Banach space of all linear bounded maps from X to Y. Suppose $(x_0, \lambda_0) \in X \times \mathbb{R}$ solves $g(x, \lambda) = 0$. If $(D_x g(x_0, \lambda_0))^{-1} : Y \to X$ exists and is in $\mathcal{L}(Y, X)$, as a consequence of the implicit function theorem, there are small $\delta > 0$ and a function $\tilde{x} : (\lambda_0 - \delta, \lambda_0 + \delta) \to X$ such that $g(\tilde{x}(\lambda), \lambda) = 0$ for all λ in the interval. Moreover (x_0, λ_0) can serve as a good initial guess for solving $g(x, \lambda) = 0$ using the Newton's method when λ is close to λ_0. To be more precise, we employ the iteration scheme

$$x_{n+1} = x_n - (D_x g(x, \lambda))^{-1} g(x_n, \lambda), \qquad n = 0, 1, 2, ...$$

Suppose $\{u_n\}$ converges, then $\tilde{u}(\lambda) \equiv \lim u_n$ is the sought-after solution for λ. One can repeat this procedure when we change λ gradually to find the solution curve as long as $(D_x g(x, \lambda))^{-1}$ exists. The solution curve in the (u, λ) space is known as the bifurcation diagram.

When the solution curve at (x, λ) forms a fold, $(D_x g(x_1, \lambda_1))^{-1}$ does not exist at the turning point and the above Newton's method fails. In our circumstances we can remedy this by using the following continuation algorithm.

3.2.1 Before engaging the continuation algorithm

Before we start the continuation algorithm, we use the steepest descent method to compute x_0 when $\lambda = \lambda_0$. Let $s = s_0$ at this location (without loss of generality we can set $s_0 = 0$). Assume $(D_x g)^{-1}(x_0, \lambda_0)$ exists. Since $g(x(s), \lambda(s)) = 0$, we differentiate to obtain

$$D_x g(x, \lambda) \cdot \frac{dx}{ds} + D_\lambda g(x, \lambda) \cdot \frac{d\lambda}{ds} = 0. \tag{3.2.1}$$

Using an overdot to represent the derivative with respect to s, it follows that

$$\dot{x} = -(D_x g)^{-1}(D_\lambda g)\dot{\lambda}. \tag{3.2.2}$$

Define

$$\widetilde{N}(x, \lambda, s) \equiv \left\| \frac{dx}{ds} \right\|^2 + \left| \frac{d\lambda}{ds} \right|^2 - 1, \tag{3.2.3}$$

where $\| \cdot \|$ is the norm in X. From the definition of arc length, we impose the constraint $\widetilde{N} = 0$. Combine with (3.2.2) we have

$$\dot{\lambda}^2 \left(1 + \left\| (D_x g)^{-1} D_\lambda g \right\|^2 \right) = 1. \tag{3.2.4}$$

This gives

$$|\dot{\lambda}| = \left(1 + \left\| (D_x g)^{-1} D_\lambda g \right\|^2 \right)^{-\frac{1}{2}}. \tag{3.2.5}$$

At $s = s_0 = 0$, we choose $\dot{\lambda}(s_0) > 0$ if we want λ to increase initially. Similarly we impose $\dot{\lambda}(s_0) < 0$ if λ decreases initially. Hence $\dot{\lambda}(s_0)$ is determined and we can evaluate $\dot{x}(s_0)$ from (3.2.2).

Take a λ_1 which is close to λ_0. Suppose for simplicity $\lambda_1 > \lambda_0$ so that we choose

$\dot{\lambda}(s_0) > 0$. With $\dot{\lambda}(s_0)$ known, we can compute Δs from

$$\lambda_1 = \lambda_0 + \dot{\lambda}(s_0) \cdot \Delta s. \tag{3.2.6}$$

Let $x = x_1$ be a solution close to x_0 and satisfy $g(x_1, \lambda_1) = 0$. To compute x_1, we employ the initial guess

$$x_1^{(0)} = x_0 + \dot{x}(s_0) \cdot \Delta s, \tag{3.2.7}$$

which will be a better choice than x_0. Assuming $(D_x g(x_1, \lambda_1))^{-1}$ exists, the Newton's method

$$x_1^{(m+1)} = x_1^{(m)} - (D_x g(x_1^{(m)}, \lambda_1))^{-1} \cdot g(x_1^{(m)}, \lambda_1), \quad m = 0, 1, 2, ... \tag{3.2.8}$$

will converge to the solution x_1. This solution (x_1, λ_1) corresponds to $s = s_1 \equiv s_0 + \Delta s$.

Algorithm (Finding the first 2 adjacent solutions)

1.Find x_0 for a given λ_0 so that $g(x_0, \lambda_0) = 0$ using steepest descent algorithm in Chapter 1. We assign $s = s_0 = 0$ for this solution.

2. Calculate $D_\lambda g(x(0), \lambda(0))$ and $D_x g(x(0), \lambda(0))$.

3. Solve $D_x g(x(0), \lambda(0)) Z = D_\lambda g(x(0), \lambda(0))$.

4. Given another nearly λ_1, we take $\text{sign}(\dot{\lambda}(0)) = \text{sign}(\lambda_1 - \lambda_0)$.

5. $\dot{\lambda}(0) = \text{sign}\ (\dot{\lambda}(0))\ (1 + \|Z\|^2)^{-\frac{1}{2}}$.

6. Calculate $\dot{x}(0) = -\dot{\lambda}(0) Z$.

7. Compute Δs by (3.2.6)

8. Use (3.2.7) to calculate an initial guess of x_1. Iterate using (3.2.8).

9. Set $s_1 = s_0 + \Delta s = \Delta s$ for the solution (x_1, λ_1).

10- Employ the continuation algorithm to be described next.

3.2.2 The continuation algorithm

In the continuation algorithm, we think of (x, λ) as parameterized by the arc length s along the solution curve. First we augment the original equation $g(x, \lambda) = 0$ with the scalar equation $\widetilde{N}(x, \lambda, s) = 0$ where $\widetilde{N}$ has been defined in (3.2.3). Let

$$\widetilde{G}(x, \lambda, s) \equiv \begin{pmatrix} g(x, \lambda) \\ \widetilde{N}(x, \lambda, s) \end{pmatrix} \tag{3.2.9}$$

so that $\widetilde{G} : X \times \mathbb{R} \times \mathbb{R} \to Y \times \mathbb{R}$. We already know $G(x_0, \lambda_0, s_0) = G(x_1, \lambda_1, s_1) = 0$. Choose a small $\Delta s > 0$ and let

$$s_{i+1} = s_i + \Delta s \ , \quad i = 1, 2, 3, ... \quad .$$

Suppose $(D_{(x,\lambda)}\widetilde{G}(x_1, \lambda_1, s_1))^{-1} \in \mathcal{L}(Y \times \mathbb{R}, X \times \mathbb{R})$, then $x = \widetilde{x}(s)$ and $\lambda = \widetilde{\lambda}(s)$ for some function $\widetilde{x}$ and $\widetilde{\lambda}$ in a neighborhood of $s = s_2$. We can now use the Newton's method on this larger system $\widetilde{G} = 0$ with some appropriate initial guess (x, λ).

3.2.3 Pseudo arc length continuation

To facilitate computation, we employ a slight modification of the above continuation algorithm, which is known as the pseudo arc length parametrization. Suppose $(x(s), \lambda(s))$ are known at $s = s_{k-1}$ and $s = s_k$. Define

$$N(x, \lambda, s) \equiv \dot{x}(s_k) \cdot (x(s) - x(s_k)) + \dot{\lambda}(s_k) \cdot (\lambda(s) - \lambda(s_k)) - \Delta s. \tag{3.2.10}$$

From the definition of arc length along the solution curve in the (x, λ) space, we need to impose

$$\left\| \frac{dx}{ds} \right\|^2 + \left| \frac{d\lambda}{ds} \right|^2 = 1. \tag{3.2.11}$$

To calculate $\frac{dx}{ds}(s_k)$ and $\frac{d\lambda}{ds}(s_k)$, we let

$$z = \frac{1}{\Delta s} \left(x(s_k) - x(s_{k-1}), \lambda(s_k) - \lambda(s_{k-1}) \right) \tag{3.2.12}$$

so that

$$\|z\| = \frac{1}{\Delta s} \sqrt{\|x(s_k) - x(s_{k-1})\|^2 + |\lambda(s_k) - \lambda(s_{k-1})|^2}. \tag{3.2.13}$$

It is clear that $\frac{z}{\|z\|}$ represents an approximation to $\left(\frac{dx}{ds}(s_k), \frac{d\lambda}{ds}(s_k) \right)$ while preserving (3.2.11). Instead of finding solution of $\widetilde{G} = 0$, we let

$$G(x, \lambda, s) \equiv \begin{pmatrix} g(x, \lambda) \\ N(x, \lambda, s) \end{pmatrix} \tag{3.2.14}$$

and look for solution of $G = 0$ at $s = s_{k+1}$. Even if $(D_x g)^{-1}$ does not exist at this point, one can still have the existence of $(D_{(x,\lambda)} G)^{-1}$. Therefore we can employ the Newton's method on the extended system:

$$(x^{(i+1)}, \lambda^{(i+1)}) = (x^{(i)}, \lambda^{(i)}) - (D_{(x,\lambda)} G)^{-1}(x^{(i)}, \lambda^{(i)}, s_{k+1}) G(x^{(i)}, \lambda^{(i)}, s_{k+1}), \quad i = 0, 1, 2, ... \tag{3.2.15}$$

to find the solution (x, λ) that corresponds to $s = s_{k+1}$. Here k is fixed. The choice of $(x^{(0)}, \lambda^{(0)})$ will be discussed next.

With $\frac{dx}{ds}(s_k)$ and $\frac{d\lambda}{ds}(s_k)$ being calculated by $\frac{z}{\|z\|}$ already, we let

$$\begin{aligned} x^{(0)} &\equiv x(s_k) + +\dot{x}(s_k)(s_{k+1} - s_k), \\ \lambda^{(0)} &\equiv \lambda(s_k) + \dot{\lambda}(s_k)(s_{k+1} - s_k). \end{aligned}$$

Then $(x^{(0)}, \lambda^{(0)})$ serves as initial guess to solve (3.2.14) for $s = s_{k+1}$.

3.3 Asymptotic boundary conditions

The asymptotic boundary conditions for the continuation method differ from those for the steepest descent algorithm. As $x \to \infty$, both a pulse and front satisfy $(u, v) \to (0, 0)$; their asymptotic behavior are therefore similar and give rise to the same asymptotic boundary conditions. On the other hand as $x \to -\infty$, their behaviors differ.

3.3.1 At $x = \infty$ (for both pulse and front)

Let $a >> 1$. On the interval $[a, \infty)$, we linearize (3.1.4a)-(3.1.4b) about $(u, v) = (0, 0)$ and obtain

$$c_0^2 \begin{pmatrix} \widetilde{u} \\ \widetilde{v} \end{pmatrix}_{xx} + c_0^2 \begin{pmatrix} \widetilde{u} \\ \widetilde{v} \end{pmatrix}_{x} - A \begin{pmatrix} \widetilde{u} \\ \widetilde{v} \end{pmatrix} = 0, \tag{3.3.1}$$

where $A = \begin{pmatrix} \frac{\beta}{d} & \frac{1}{d} \\ -1 & \gamma \end{pmatrix}$. Note that $(\widetilde{u}, \widetilde{v})$ is a good approximation of (u, v) for large x. When d is sufficiently small, the matrix A has 2 real and positive eigenvalues

$0 < \lambda_1 < \lambda_2$ that satisfy

$$d\lambda^2 - (\beta + d\gamma)\lambda + (1 + \gamma\beta) = 0. \tag{3.3.2}$$

Moreover (see [2])

$$0 < \lambda_1 < \frac{\beta}{2d} < \frac{1}{2}\left(\gamma + \frac{\beta}{d}\right) < \lambda_2 < \frac{\beta}{d}. \tag{3.3.3}$$

In addition, by (3.3.3)

$$\gamma < \frac{\beta}{d}. \tag{3.3.4}$$

Let $\vec{a}$, $\vec{b}$ be the eigenvectors corresponding to eigenvalues λ_1 and λ_2, respectively. Define $\alpha_2 = \frac{\beta}{d} - \lambda_1$, which is positive by (3.3.3). It is readily checked that $\vec{a} = \begin{pmatrix} -1 \\ d\alpha_2 \end{pmatrix}$ and $\vec{b} = \begin{pmatrix} -\alpha_2 \\ 1 \end{pmatrix}$.

Denote by s_2, s_3 the roots of $s^2 + s - \dfrac{\lambda_1}{c^2} = 0$ and s_1, s_4 those of $s^2 + s - \dfrac{\lambda_2}{c^2} = 0$. One verifies

$$s_1 < s_2 < -1 < 0 < s_3 < s_4.$$

By restricting to bounded solution of $(\widetilde{u}, \widetilde{v})$ for (3.3.1) (see Lemma 6.1 in [2]), we have

$$\begin{pmatrix} u \\ v \end{pmatrix} \sim \begin{pmatrix} \widetilde{u} \\ \widetilde{v} \end{pmatrix} = D_1 \vec{b} e^{s_1 x} + D_2 \vec{a} e^{s_2 x} \quad \text{as } x \to \infty, \tag{3.3.5}$$

where D_1 and D_2 are some constants (see [2]). It has been shown that $D_2 \neq 0$. With

$s_1 < s_2 < 0$ the above asymptotic relation simplifies to

$$\begin{pmatrix} u \\ v \end{pmatrix} \sim D_2 \vec{a} s_2 e^{s_2 x} \quad \text{as } x \to \infty. \tag{3.3.6}$$

Moreover

$$\begin{pmatrix} u \\ v \end{pmatrix}' \sim D_2 \vec{a} s_2 e^{s_2 x} \quad \text{as } x \to -\infty. \tag{3.3.7}$$

Hence $u' \sim s_2 u$ and $v' \sim s_2 v$ as $x \to \infty$. We therefore impose the asymptotic boundary conditions $u' = s_2 u$ and $v' = s_2 v$ at $x = x_N$.

3.3.2 At $x = -\infty$ for the pulse

Following the similar derivation in (3.3.1) we have

$$\begin{pmatrix} u \\ v \end{pmatrix} \sim C_1 \vec{b} e^{s_4 x} + C_2 \vec{a} e^{s_3 x} \quad \text{as } x \to -\infty, \tag{3.3.8}$$

where C_1 and C_2 are constants. Again it can be shown that $C_2 \neq 0$. With $s_4 > s_3 > 0$, it follows that

$$\begin{pmatrix} u \\ v \end{pmatrix} \sim C_2 \vec{a} s_3 e^{s_3 x} \quad \text{as } x \to -\infty. \tag{3.3.9}$$

Moreover

$$\begin{pmatrix} u \\ v \end{pmatrix}' \sim C_2 \vec{a} s_3 e^{s_3 x} \quad \text{as } x \to -\infty. \tag{3.3.10}$$

We therefore impose the asymptotic boundary conditions $u' = s_3 u$ and $v' = s_3 v$ at $x = x_0$.

3.3.3 At $x = -\infty$ for the front

In this case $(u, v) = (\mu_3, \frac{\mu_3}{\gamma})$ as $x \to -\infty$. Let $a >> 1$. With (U, V) as in Section 1.4, by linearization about this equilibrium solution, it is known that

$$-\begin{pmatrix} U \\ V \end{pmatrix} = \begin{pmatrix} u - \mu_3 \\ v - \frac{\mu_3}{\gamma} \end{pmatrix} \sim \begin{pmatrix} \widetilde{u} \\ \widetilde{v} \end{pmatrix} \text{ as } x \to -\infty$$

with

$$c_0^2 \begin{pmatrix} \widetilde{u} \\ \widetilde{v} \end{pmatrix}_{xx} + c_0^2 \begin{pmatrix} \widetilde{u} \\ \widetilde{v} \end{pmatrix}_{x} - \widehat{A} \begin{pmatrix} \widetilde{u} \\ \widetilde{v} \end{pmatrix} = 0 \qquad \text{on } (-\infty, -a] \tag{3.3.11}$$

and $\widehat{A} = \begin{pmatrix} \frac{-f'(\mu_3)}{d} & \frac{1}{d} \\ -1 & \gamma \end{pmatrix}$. When d is sufficiently small, this matrix has 2 real and positive eigenvalues $0 < \widehat{\lambda}_1 < \widehat{\lambda}_2$ that satisfy

$$d\widehat{\lambda}^2 + (f'(\mu_3) - d\gamma)\widehat{\lambda} + (1 - \gamma f'(\mu_3)) = 0. \tag{3.3.12}$$

Denote by $\widehat{s}_2$, $\widehat{s}_3$ the roots of $s^2 + s - \frac{\widehat{\lambda_1}}{c^2} = 0$ and s_1, s_4 those of $s^2 + s - \frac{\widehat{\lambda_2}}{c^2} = 0$. It is readily checked that

$$\widehat{s}_1 < \widehat{s}_2 < -1 < 0 < \widehat{s}_3 < \widehat{s}_4.$$

A similar analysis gives $U' \sim \widehat{s}_3 U$ and $V' \sim \widehat{s}_3 V$, as $x \to -\infty$. We therefore impose the asymptotic boundary conditions $U' = \widehat{s}_3 U$ and $V' = \widehat{s}_3 V$ at $x = x_0$.

3.4 Discretization of the governing equations

The governing equations for the pseudo arc length continuation method are given by $G = 0$ in (3.2.14), where g has been defined in (3.1.5). Again we use $[a, b]$ to approximate $(-\infty, \infty)$ with $x_0 = a$, $x_N = b$, and $x_j - x_{j-1} = h = \frac{b-a}{N}$ for $j = 1, 2, ..., N$. For (3.1.4a) we employ the finite difference approximation:

$$u''|_{x_i} = \frac{1}{12\Delta x^2}(-u_{i+2} + 16u_{i+1} - 30u_i + 16u_{i-1} - u_{i-2}),\ i = 2, 3, ..., N-2,$$

$$u'|_{x_i} = \frac{1}{12\Delta x}(-u_{i+2} + 8u_{i+1} - 8u_{i-1} + u_{i-2}),\ i = 2, 3, ..., N-2,$$

for the interior nodes. Both have an accuracy of $\mathcal{O}(h^4)$, see [14]. When $i = 1$ and $i = N - 1$ we use

$$u''|_{x_1} = \frac{1}{12\Delta x^2}(10u_0 - 15u_1 - 4u_2 + 14u_3 - 6u_4 + u_5),$$

$$u'|_{x_1} = \frac{1}{12\Delta x}(-3u_0 - 10u_1 + 18u_2 - 6u_3 + u_4),$$

$$u''|_{x_{N-1}} = \frac{1}{12\Delta x^2}(u_{N-5} - 6u_{N-4} + 14u_{N-3} - 4u_{N-2} - 15u_{N-1} + 10u_N),$$

$$u'|_{x_{N-1}} = \frac{1}{12\Delta x}(-u_{N-4} + 6u_{N-3} - 18u_{N-2} + 10u_{N-1} + 3u_N),$$

which preserve the same order of accuracy. To derive the fourth order finite difference at the boundary when $i = 0$ we examine the Taylor expansion

$$u_k = u_0 + khu_0' + \frac{k^2h^2}{2!}u_0'' + \frac{k^3h^3}{3!}u_0^{(3)} + \frac{k^4h^4}{4!}u_0^{(4)} + \mathcal{O}(h^5)\ \ k = 1, ..., 4. \qquad (3.4.1)$$

Now put $u'|_{x_0} = s_3 u_0$ in (3.4.1). Using various u_k for $k = 1, 2, 3, 4$, we can eliminate $u_0^{(3)}$ and $u_0^{(4)}$, this leads to the $\mathcal{O}(h^5)$ finite difference formula at $x = x_0$

$$u''|_{x_0} = \frac{2}{h^2}\left(\left(\frac{-25}{12}hs_3 - \frac{415}{144}\right)u_0 + 4u_1 - \frac{3}{2}u_2 + \frac{4}{9}u_3 - \frac{1}{16}u_4\right).$$

A similar analysis using $u'|_{x_N} = s_2 u_N$ in (3.4.1) gives

$$u''|_{x_N} = \frac{2}{h^2}\left(\left(\frac{25}{12}hs_2 - \frac{415}{144}\right)u_N + 4u_{N-1} - \frac{3}{2}u_{N-2} + \frac{4}{9}u_{N-3} - \frac{1}{16}u_{N-4}\right).$$

The same derivation is applicable to v in (3.1.4b). The last equation (3.1.4c) involves numerical quadrature. With $f(x) = u'^2 + u^2$, we apply the composite Simpson's rule

$$\int_a^b f(x)dx \approx \frac{h}{3}\sum_{i=1}^{\frac{N-1}{2}}\left(f(x_{2i-1}) + 4f(x_{2i}) + f(x_{2i+1})\right) \tag{3.4.2}$$

to compute

$$\int_{-\infty}^{\infty} e^x(u'^2 + u^2)dx.$$

As is well-known, the quadrature error for simpson's rule is $\mathcal{O}(h^4)$.

Chapter 4

Numerical results

In this chapter we report numerical results obtained using algorithms documented earlier. It is remarkable that for some suitable range of (d, γ, β), we find at least 5 traveling wave solutions with distinct wave speeds.

4.1 Numerical results of the steepest descent algorithm

In the steepest descent algorithm we look for minimizers in some admissible set. The admissible sets for the pulse and the front are $\mathcal{A}_p$ and $\mathcal{A}_f$, respectively, defined in Chapter 1. A good initial guess of the (u, v, c) is not required for the convergence of the algorithm. We fix $\beta = 0.25$ $\gamma = 8.6984$ and allow d to vary. For this β, the constraint (1.1.1) becomes $7.1111 < \gamma < 10.2857$ so that the prescribed γ lies inside this range. For all our numerical experiments using the steepest descent, we use a mesh size $5.0e-3$ on the computational domain $= [-110, 40]$ to approximate

$(-\infty, \infty)$; the number of grid points are 30001 points in our numerical experiments for both pulse and fronts.

When d is large, there is no traveling wave solution. For small d we find both traveling pulses and fronts.

4.1.1 Case 1: Pulses

Let $d = 1.8e-3$ in our initial set of experiments. For each $c > 0$, we find a minimizer u_c of J_c using the steepest descent algorithm. As already defined in Chapter 1, we let $\mathcal{J}(c) \equiv J_c(u_c) = \min_{u \in \mathcal{A}_p} J_c(u)$. A plot of $\mathcal{J}$ versus c for this value of d is given in Figure 4.1.1. We see that $\mathcal{J}$ has no root so that there is no traveling pulse solution within the confine of $\mathcal{A}_p$.

We now make d slightly smaller at $1.6e-3$. The results are also given in Figure 4.1.1. There are two roots of $\mathcal{J} : c = c_0 \cong 4.98$ and $c = c_1 \cong 2$. Let u_0 and u_1 be the corresponding minimizers associated with $c = c_0$ and $c = c_1$ respectively. Then $(u_0, \mathcal{L}_{c_0} u_0, c_0)$ and $(u_1, \mathcal{L}_{c_1} u_1, c_1)$ are traveling pulse solutions in the admissible set $\mathcal{A}_p$. Hence there are two of them for the same γ, β and this d.

As we push d progressively smaller, we see that $c_1 \to 0$ at some finite d, leaving behind only one traveling pulse. This can be clearly seen when $d = 5.0e-4$. There is only one $c = c_0 = 14.3$ where $\mathcal{J}(c) = 0$. Thus $(u_0, \mathcal{L}_{c_0} u_0, c_0)$ is a traveling pulse for this value of d. Additional results are tabulated in Tables 4.1.1. For all such d, we have only one unique traveling pulse.

We now document the shapes of traveling pulses. When $d = 1.6e-3$, we have two pulses with distinct speeds $0 < c_1 < c_0$. Using $v_i = \mathcal{L}_{c_i} u_i$ for $i = 0, 1$, the solutions (u_0, v_0) and (u_1, v_1) are given in Figures 4.1.2 and 4.1.3, respectively. In Figure 4.1.4

d	c	$\min(u)$	$\max(v)$	dc^2
$5.0e-4$	14.3	-0.1458	0.0796	0.1022
$4.23e-4$	15.8	-0.1486	0.0798	0.1056
$3.0e-4$	19.27	-0.1536	0.0802	0.1114
$1.0e-4$	34.71	-0.1612	0.0803	0.1205

TABLE 4.1.1: traveling pulse for $\beta = 0.25$ and $\gamma = 8.6984$.

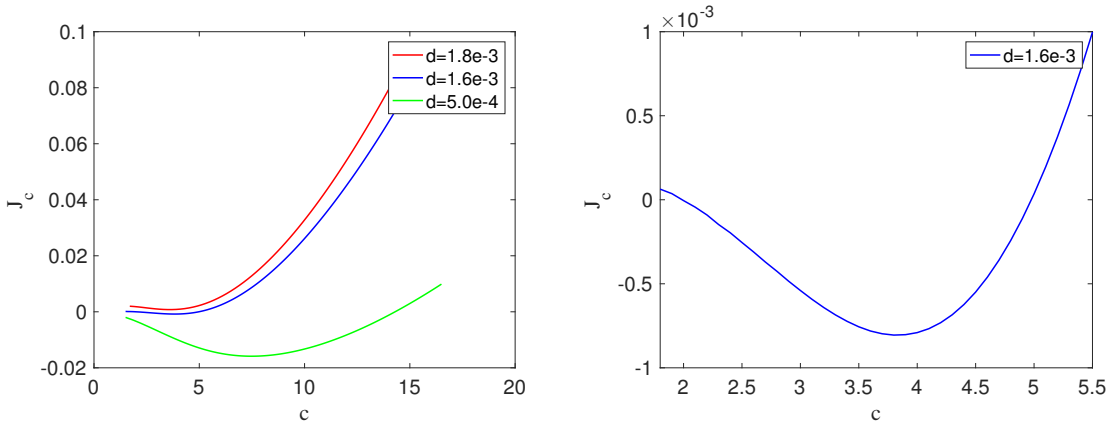

FIGURE 4.1.1: A plot of $\mathcal{J}$ vs. c when $\beta = 0.25$ and $\gamma = 8.6984$ for traveling pulse. Each curve corresponds to the indicated d. The right picture a plot of $\mathcal{J}$ vs. c when $\beta = 0.25$, $d = 1.6e-3$ and $\gamma = 8.6984$. There are two roots of $\mathcal{J} : c = c_0 \cong 4.98$ and $c = c_1 \cong 2$.

we overlay the solutions u_0 and u_1 to explore their differences in shape. It is clear that the pulse width associated with the faster wave is significantly larger. In the same figure we also compare the profiles of v_0 and v_1.

Inputing these profiles as initial conditions for the parabolic solver of (1.1.2), we record the successive wave profiles of various time intervals in Figure 4.1.5. It shows that the wave corresponding to $c = c_0$ keeps the same shape and moves with a speed c_0. This indicates this wave is stable. To substantiate this claim, we plot the final u profile at $t = 7.5$ from the parabolic solvers side by side with u_0 from the steepest descent algorithm in the left picture of Figure 4.1.7. The two profiles are in fact

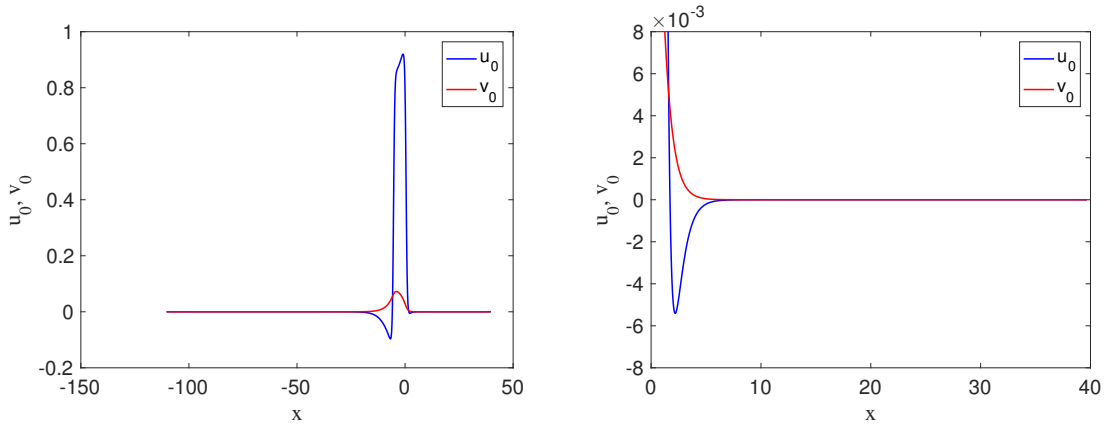

FIGURE 4.1.2: traveling pulse with speed $c_0 \cong 4.98$ when $\beta = 0.25$, $\gamma = 8.6984$ and $d = 1.6e-3$. The right picture is magnified view of the left in the leading edge of the traveling wave.

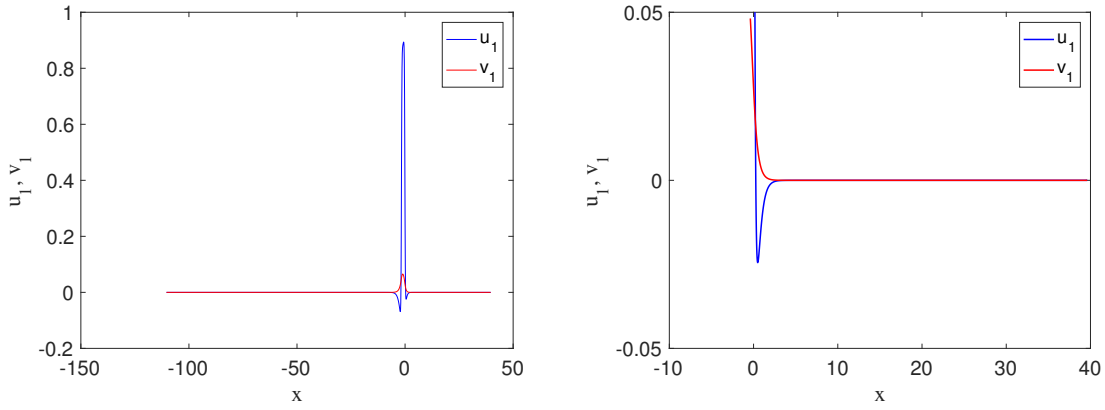

FIGURE 4.1.3: traveling pulse with speed $c_1 \cong 2$ when $\beta = 0.25$, $\gamma = 8.6984$ and $d = 1.6e-3$. The right picture is magnified view of the left in the leading edge of the traveling wave.

indistinguishable in the picture.

We do the same on the wave for $c = c_1$. However this time the wave rapidly breaks up and reorganizes as the fast stable wave profile seen in Figure 4.1.6. A comparison of the final u profile of $t = 7.5$ with that of u_0 is given on the right picture of Figure 4.1.7. The slow wave is therefore unstable.

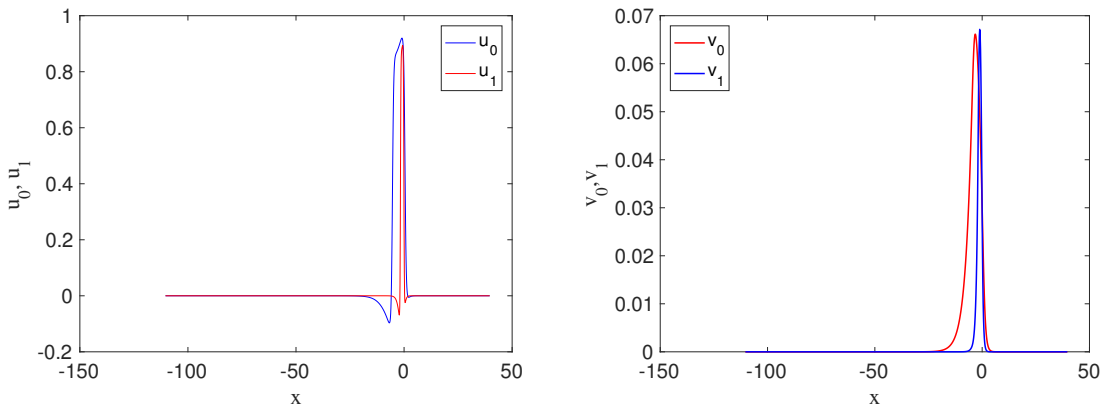

FIGURE 4.1.4: Difference in shapes between u_0 and u_1, and between v_0 and v_1 for traveling pulse.

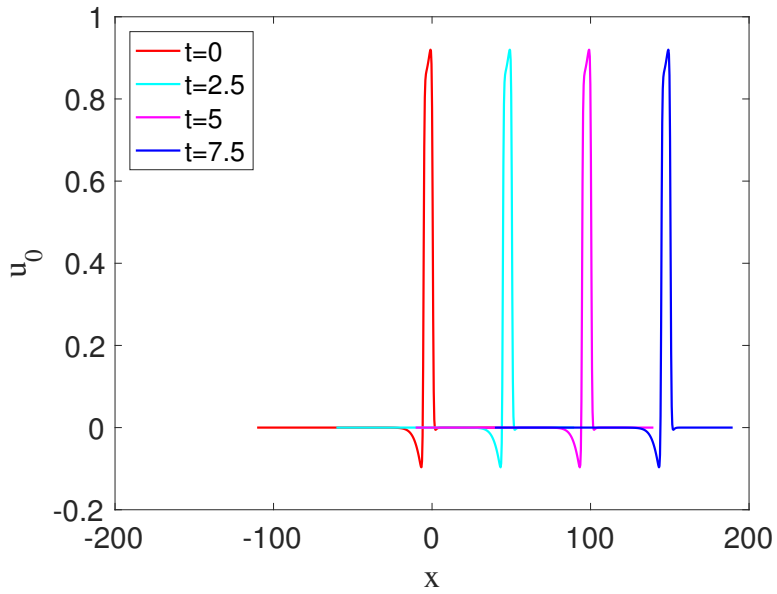

FIGURE 4.1.5: The fast moving pulse travels at constant speed c_0 when the profile in figure 4.1.2, obtained by steepest descent algorithm, is input as initial conditions in the parabolic solvers.

Finally we investigate the change in the fast pulse profile with respect to d in Figure 4.1.8. We see that as d decreases, the pulse width increases rapidly while

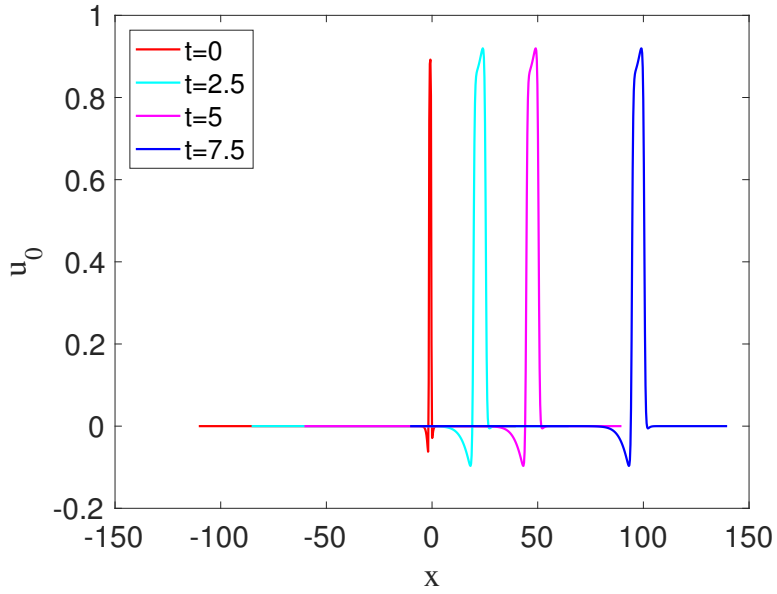

FIGURE 4.1.6: The slow moving pulse breaks up and evolves into the fast moving pulse when the profile in Figure 4.1.3, obtained by steepest descent algorithm, is input as initial conditions in the parabolic solvers.

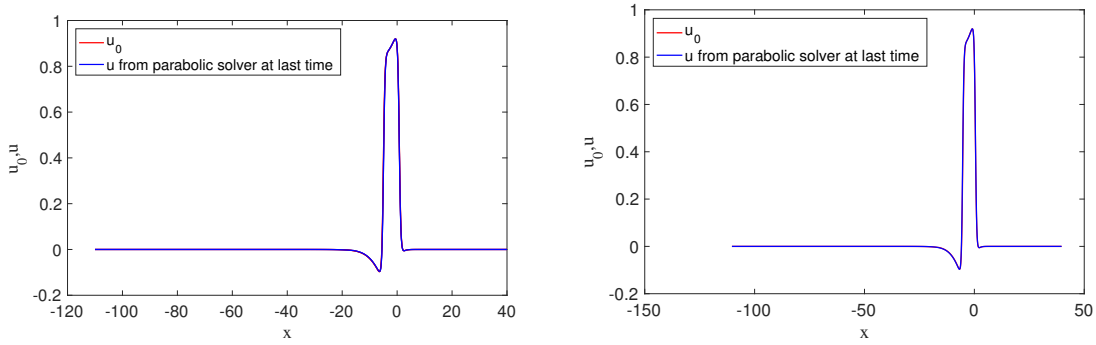

FIGURE 4.1.7: The parabolic solver solution at $t = 7.5$ in Figure 4.1.5 and u_0 are indistinguishable on the left picture. The same is true for the parabolic solver solution in Figure 4.1.6 and u_0 on the right.

retaining the same qualitative shape.

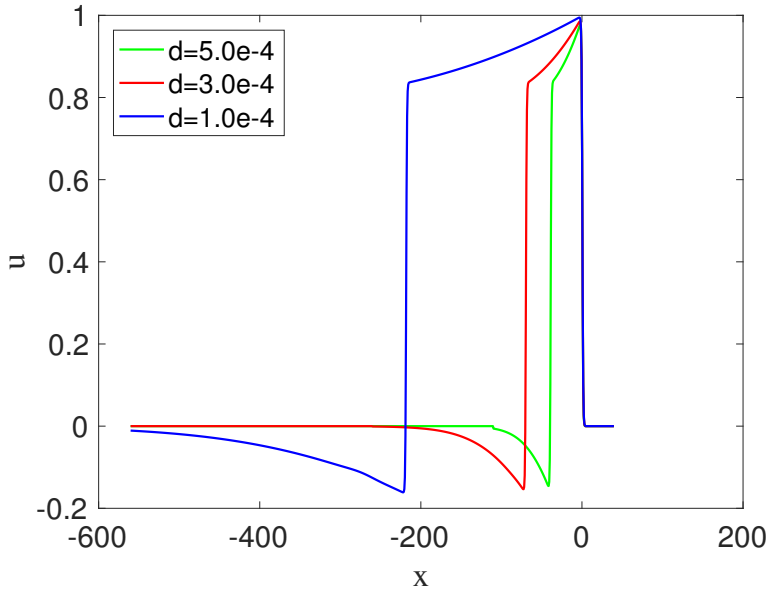

FIGURE 4.1.8: Compare profile of u for fast pulse at different d.

4.1.2 Case 2: Front moving to the right

We start with $d = 1.8e-3$ as in Case 1. For each $c > 0$, we find a minimizer u_c of J_c using the steepest descent algorithm and let $\mathcal{J}(c) \equiv J_c(u_c) = \min_{u \in \mathcal{A}_f} J_c(u)$. A plot of $\mathcal{J}$ versus c for this value of d is given in Figure 4.1.9. We see that $\mathcal{J}$ has no root so that there is no traveling front solution that moves to the right.

The numerical results for $d = 1.6e-3$ is also given in Figure 4.1.9. There are two roots of $\mathcal{J}$: $c = c_0 \cong 4.975$ and $c = c_1 \cong 2.983$. Let u_0 and u_1 be the corresponding minimizers associated with $c = c_0$ and $c = c_1$, respectively. Hence we have two right-moving traveling front solutions in the admissible set $\mathcal{A}_f$.

A similar phenomenon as in Case 1 occurs when we push d smaller. We see that $c_1 \to 0$ at some finite d, leaving behind only one traveling pulse. This can be clearly seen when $d = 1.0e-4$. There is only one $c = c_0 = 34.7$ at which $\mathcal{J}(c) = 0$. Thus

$(u_0, \mathcal{L}_{c_0} u_0, c_0)$ is a traveling front for this value of d. Restricting ourselves to the fastest traveling front, we tabulate additional numerical results see in Tables 4.1.2.

d	c_0	$\min(u)$	$\max(v)$	dc_0^2
$5.0e-4$	14.299	$-1.98e-4$	$9.01e-2$	0.1022
$4.23e-4$	15.8	$-1.37e-4$	$9.0e-2$	0.1056
$3.0e-4$	19.27	$-6.63e-5$	$8.82e-2$	0.1114
$1.0e-4$	34.71	$-6.54e-6$	$9.02e-2$	0.1205

TABLE 4.1.2: Right-moving fast traveling front for $\beta = 0.25$ and $\gamma = 8.6984$. These parameters are the same as in Table 4.1.1.

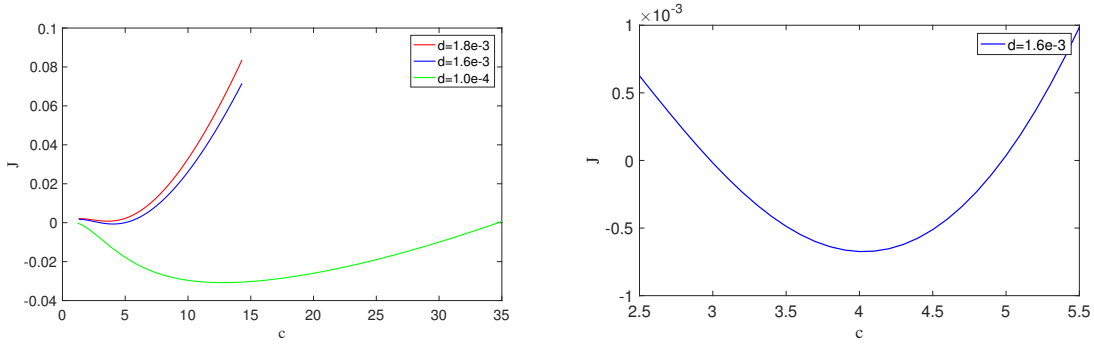

FIGURE 4.1.9: A plot of $\mathcal{J}$ vs. c when $\beta = 0.25$ and $\gamma = 8.6984$ for traveling front. Each curve corresponds to the indicated d. The right picture a plot of $\mathcal{J}$ vs. c when $\beta = 0.25$, $d = 1.6e-3$ and $\gamma = 8.6984$. There are two roots of $\mathcal{J} : c = c_0 \cong 4.975$ and $c = c_1 \cong 2.983$.

We now document the shapes of traveling pulses. When $d = 1.6e-3$, we have two pulses with distinct speeds $0 < c_1 < c_0$. Using $v_i = \mathcal{L}_{c_i} u_i$ for $i = 0, 1$, the solutions (u_0, v_0) and (u_1, v_1) are given in Figures 4.1.10 and 4.1.11, respectively. In Figure 4.1.12 we overlay the solution u_0 and u_1 to explore their differences in shape. Again the fast wave has wider front width.

Inputing these profiles as initial conditions for the parabolic solver of (1.1.2), we

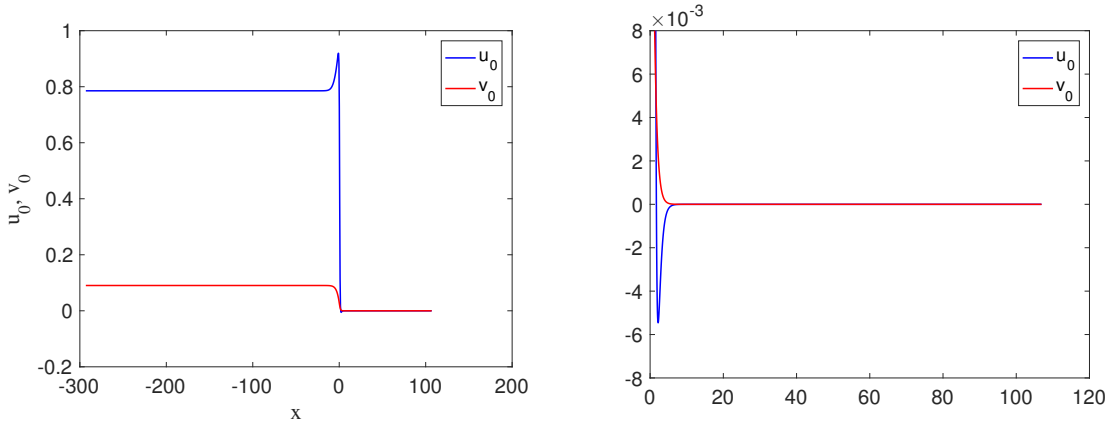

FIGURE 4.1.10: The fast right-moving traveling front with speed $c_0 \cong 4.975$ when $\beta = 0.25$, $\gamma = 8.6984$ and $d = 1.6e-3$. The right picture is magnified view of the left in the leading edge of the traveling wave.

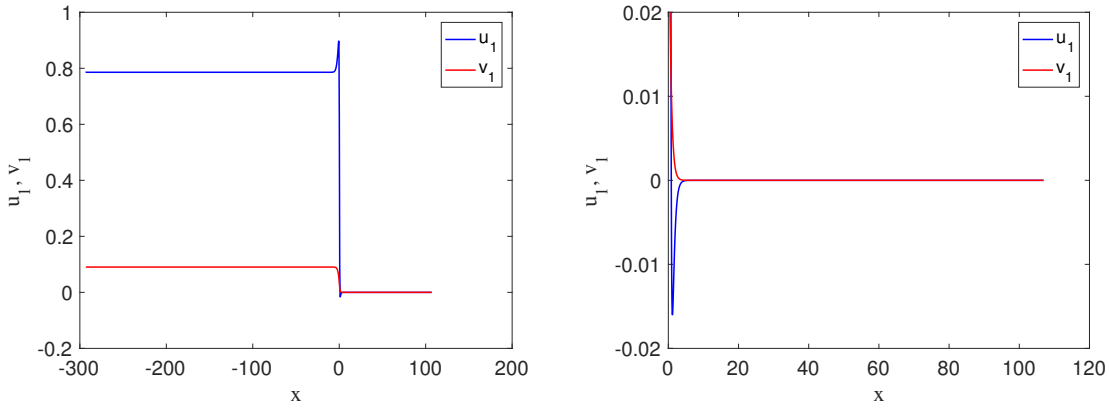

FIGURE 4.1.11: The slow right-moving traveling front with speed $c_0 \cong 2.98$ when $\beta = 0.25$, $\gamma = 8.6984$ and $d = 1.6e-3$. The right picture is magnified view of the left in the leading edge of the traveling wave.

see in Figure 4.1.13 that the wave corresponding to $c = c_0$ keeps the same shape and moves with a speed c_0. This indicates this wave is stable.

However for the wave for $c = c_1$, in Figure 4.1.14 we see that the wave rapidly breaks up and reorganizes to the fast stable wave profile. The slow wave is therefore unstable. To check that the parabolic solvers solutions evolve into u_0, we plot the

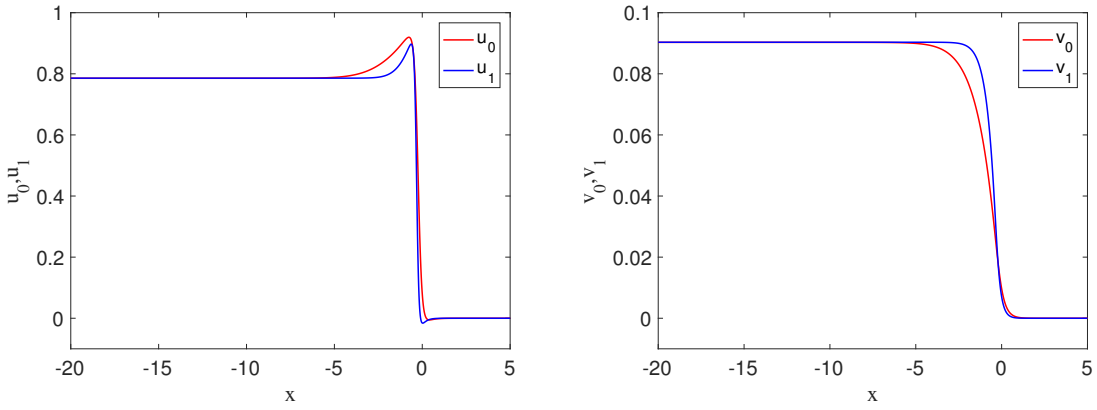

FIGURE 4.1.12: difference in shape between u_0 and u_1 and between v_0 and v_1 for right-moving traveling front.

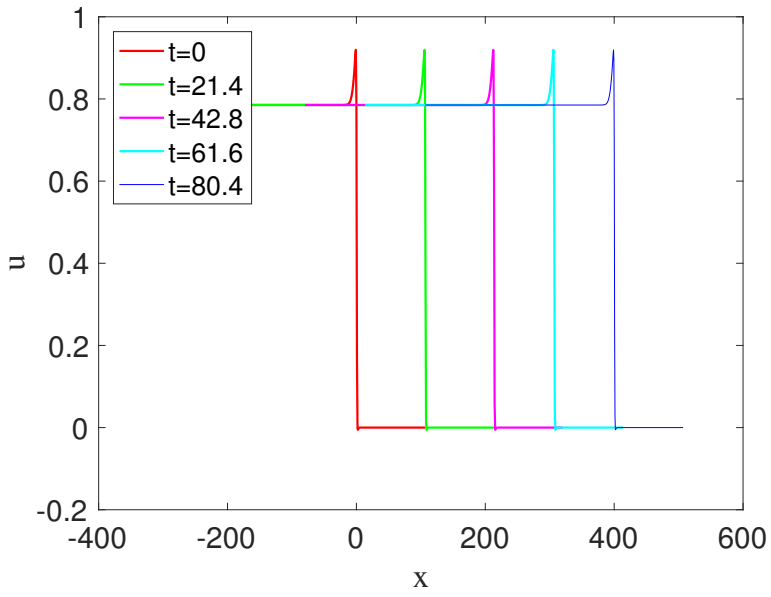

FIGURE 4.1.13: The fast right-moving front travels at constant speed c_0 when the profile in Figure 4.1.10, obtained by steepest descent algorithm, is input as initial conditions in the parabolic solvers.

solutions at final time versus u_0 in Figure 4.1.15. They indeed agree. In Figure 4.1.15 we compare the profile at last t with u_0 and u_1. Finally in Figure 4.1.16 we

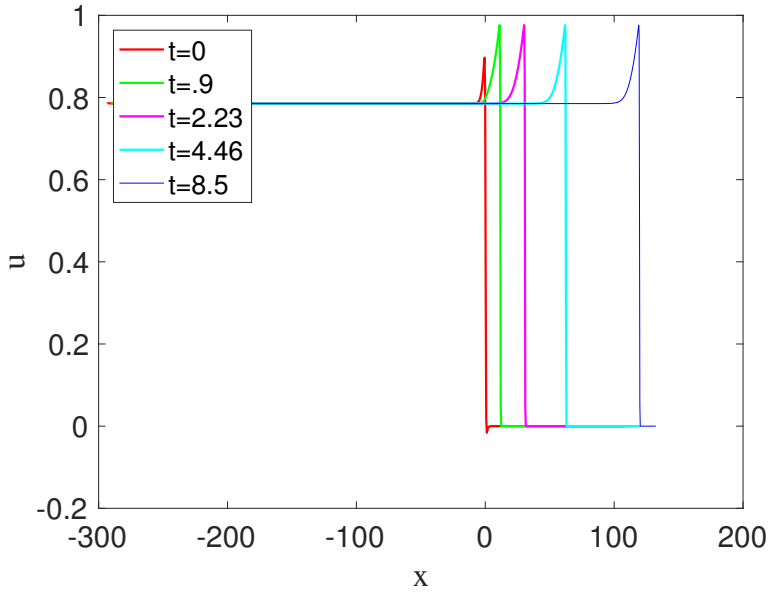

FIGURE 4.1.14: The front travels at constant speed c_1 when the profile in Figure 4.1.11, obtained by steepest descent algorithm, is input as initial conditions in the parabolic solvers.

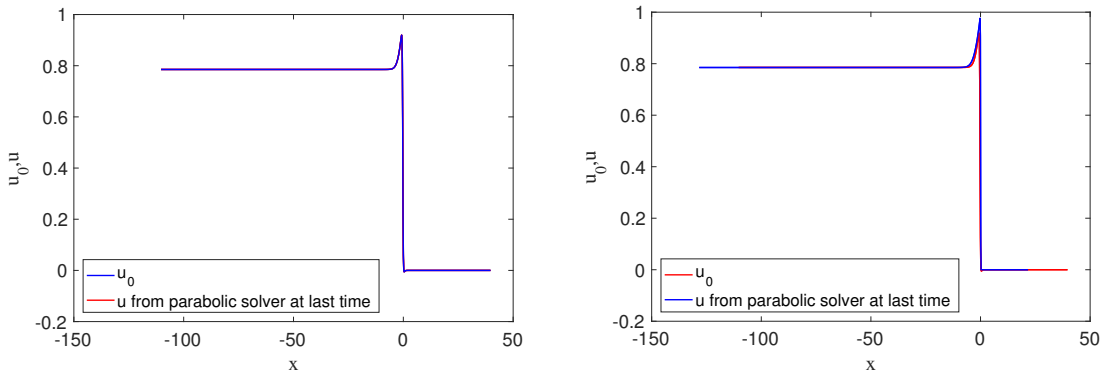

FIGURE 4.1.15: The parabolic solver solution at $t = 80.4$ in Figure 4.1.13 and u_0 are indistinguishable on the left picture. The same is true for the parabolic solver solution at $t = 8.5$ in Figure 4.1.14 and u_0 on the right.

compare the wave profiles of the fast fronts corresponding to a range of d. A smaller d gives rise to a slower decay near $x = -\infty$.

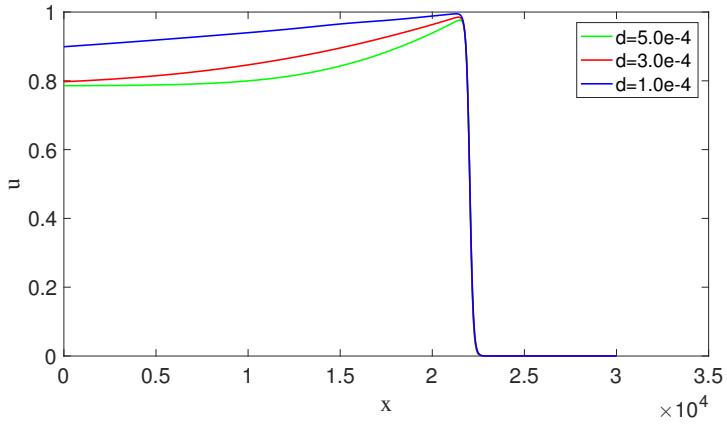

FIGURE 4.1.16: Compare profiles of u for right moving fast fronts at different d.

4.1.3 Case 3: Front moving to the left

Recall that we use the transformation $U = \mu_3 - u$ and $V = \frac{\mu_3}{\gamma} - v$ to obtain an equivalent system (1.4.2) with $(U, V) \to (0, 0)$ as $x \to \infty$ and $(U, V) \to (\mu_3, \frac{\mu_3}{\gamma})$ as $x \to -\infty$. For each $c > 0$, we find a minimizer U_c of J_c using the steepest descent algorithm. Let $\mathcal{J}(c) \equiv J_c(U_c) = \min_{U \in \mathcal{A}_f} J_c(U)$. A plot of $\mathcal{J}$ versus c for this value of d is given in Figure 4.1.17. In contrast to the other cases, $\mathcal{J}$ has at most one root. The root gives a traveling front solution $\mathcal{A}_f$ moving to the right in the (U, V) formulation. It corresponds to a front moving to the left in the original variables (u, v) . This can be clearly seen when $d = 5.0e - 4$. There is only one $c = c_0 = 20.75$ at which $\mathcal{J}(c) = 0$. Thus $(U_0, \mathcal{L}_{c_0} U_0, c_0)$ is a traveling front moving to the right for this value of d. Additional numerical results are given in the Tables 4.1.3.

After transforming back to the (u, v) variable, the wave profile is given in Figure 4.1.18. We now plot the left moving front and the 2 right moving fronts in Figure 4.1.19 to highlight their differences in shapes. Any translation of a traveling wave remains a traveling wave. But even after making a translation, the right and left

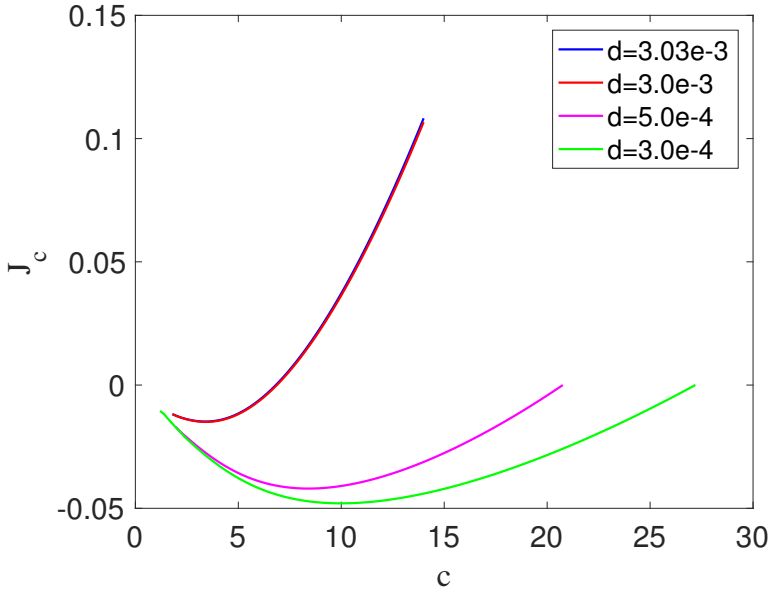

FIGURE 4.1.17: A plot of $\mathcal{J}$ vs. c when $\beta = 0.25$ and $\gamma = 8.6984$ for left moving traveling front. Each curve corresponds to the indicated d.

d	c	dc^2
$5.0e-4$	20.7597	0.2155
$3.0e-4$	27.1930	0.2218
$1.0e-4$	47.7745	0.228

TABLE 4.1.3: Left moving traveling front with $\beta = 0.25$ and $\gamma = 8.6984$. These parameters are the same as in Table 4.1.1 and 4.1.2.

moving fronts remain very different.

Next we input the (u, v) profile from the above steepest descent algorithm into the parabolic solvers. It is clear from Figure 4.1.20 that the front moves to the left with a constant speed. In Figure 4.1.21 we compare the profile at the last time $t = 7.22$ with u_0. Again the profiles are indistinguishable. Next a plot of left moving front profiles for various d are given in Figure 4.1.22. We see that a smaller d leads to a

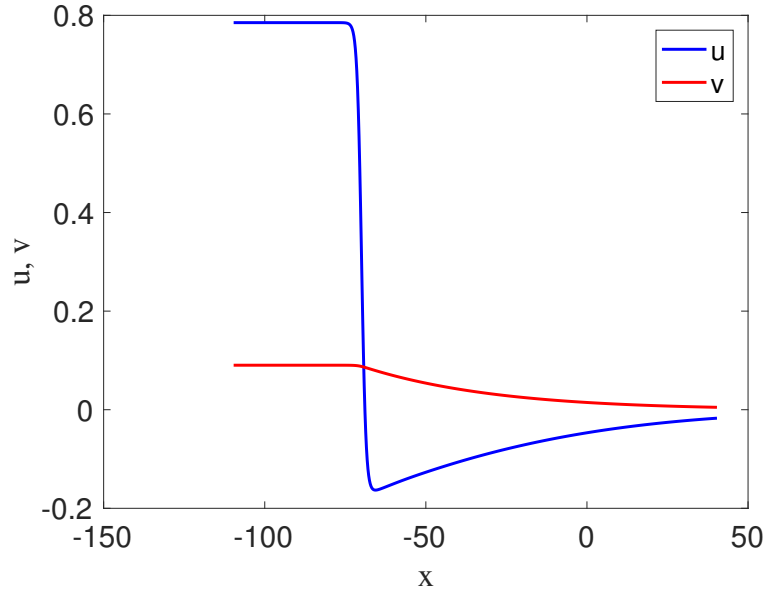

FIGURE 4.1.18: left moving traveling front with speed $c_0 \cong 20.75$ when $\beta = 0.25$, $\gamma = 8.6984$ and $d = 5.0e - 4$.

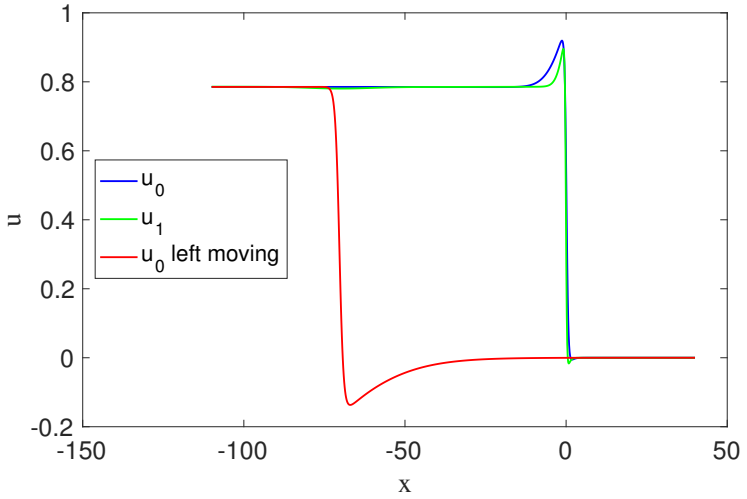

FIGURE 4.1.19: The left moving front and the 2 right moving fronts

slower decay near $x = \infty$.

For $d = 1.6e - 3$, we have therefore found 5 distinct traveling wave solutions:

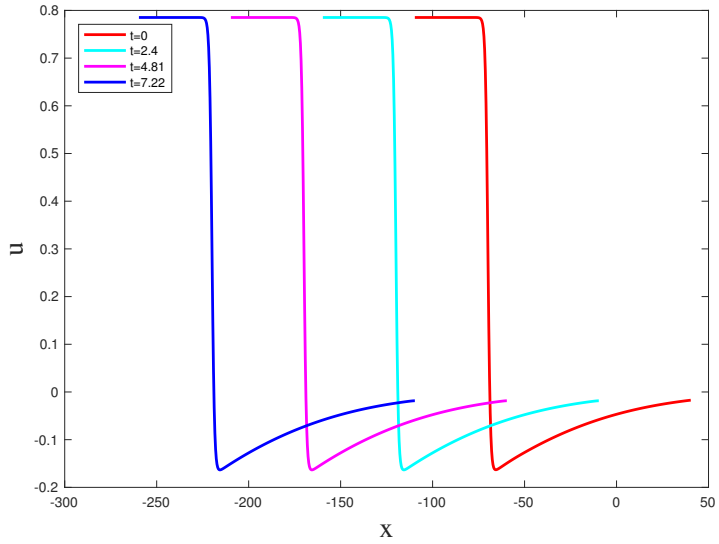

FIGURE 4.1.20: The left moving front travels at constant speed c_0 when the profile in Figure 4.1.18, obtained by steepest descent algorithm, is input as initial conditions in the parabolic solvers

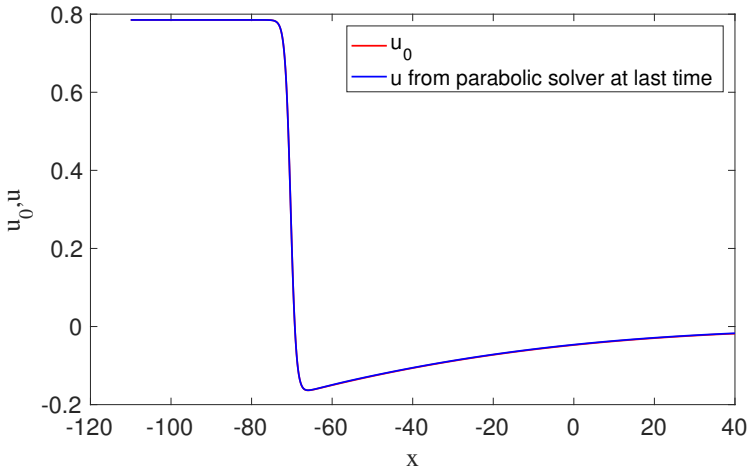

FIGURE 4.1.21: Compare the profile at last t with u_0

2 right-moving traveling pulses, 2 right-moving traveling fronts, and 1 left-moving traveling front. The u-profiles of all 5 waves are given in Figure 4.1.23

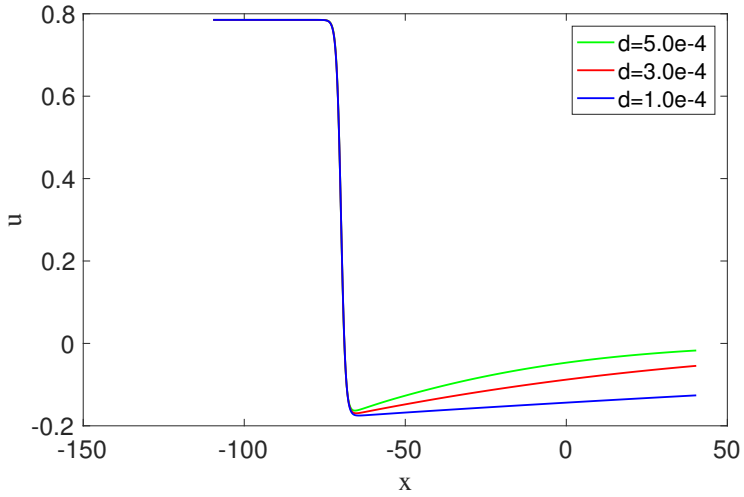

FIGURE 4.1.22: Compare profiles of left moving front u for different d.

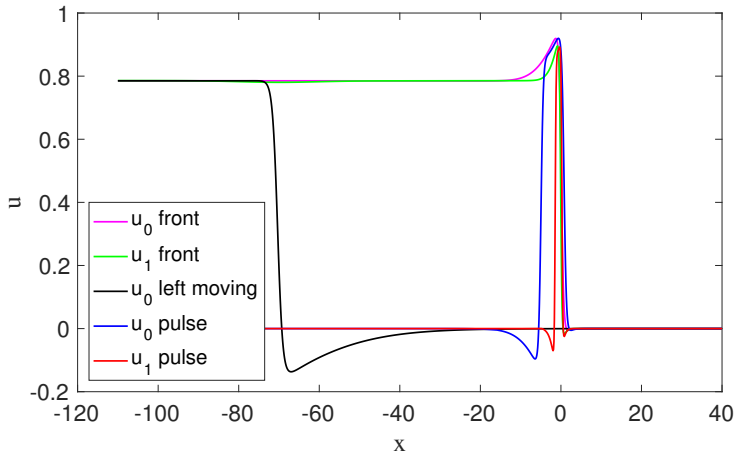

FIGURE 4.1.23: all five traveling waves when $d = 1.6e-3$, $\beta = 0.25$, and $\gamma = 8.6984$. u_0 is the fast wave and u_1 is the slow wave.

4.1.4 An independent check of our algorithm

Suppose c_p is the fastest wave speed associated with a pulse, c_{f+} is that for a front moving to the right and c_{f-} is that for a front moving to the left. It is known that both dc_p^2 and dc_{f+}^2 go to $\frac{(1-2\beta)^2}{2} = 0.125$ as $d \to 0$, see [2]. From Tables 4.1.1 and

4.1.2, our numerical results indeed validate the theoretical results. For the front traveling to the left, we have made transformation to get the governing equations (1.4.3) on (U, V), which involve the cubic polynomial nonlinearity $\widetilde{f}$. The roots of $\tilde{f}$ are $u_0 = 0$, $u_1 = 0.14174$, and $u_2 = 0.96386$. A similar argument leads to $\frac{1}{\sqrt{2dc_{f^-}^2}}(u_2 - 2u_1 + u_0) \to 1$ as $d \to 0$; in other words $dc_{f^-}^2 \to 0.231$. The results in Table 4.1.3 agree with this prediction.

4.2 Numerical results for the continuation algorithm

In Chapter 3 we have constructed a continuation algorithm which gradually adjust the physical parameters to find the bifurcation diagram. To implement this algorithm we start with the fast traveling wave solution (u, v, c) found using the steepest descent algorithm. For all our numerical experiments using the continuation method, we use a mesh size $5.0e-3$ on the computational domain $[-110, 40]$ to approximate $(-\infty, \infty)$; the number of grid points are 30001 points. We employ $\Delta s = 0.1$ in the pseudo arc length continuation algorithm described In Section 3.2.

4.2.1 Solution dependence on d

Fix $\beta = 0.25$ and $\gamma = 8.6984$ and allow d to vary. To initiate the pseudo arc length continuation method, we use the fast traveling pulse solution (u, v, c) obtained from the steepest descent algorithm. The continuation algorithm yields a bifurcation diagram whose projection on the (d, c) plane is represented in Figure 4.2.1. It is seen that there is a turning point at $d = 1.714e-3$. For $d > 1.714e-3$, there is no traveling

pulse. It is also clear that when $d < 1.714e-3$ with d being close to the turning point, there are two traveling pulses; the fast and the slow waves. Such a bifurcation diagram agrees with what we observe in the steepest descent method. It is expected that the slow wave speed c_1 goes to 0 at some finite d. However the computation for the continuation method gets increasingly difficult, therefore we cannot complete this segment of the bifurcation diagram.

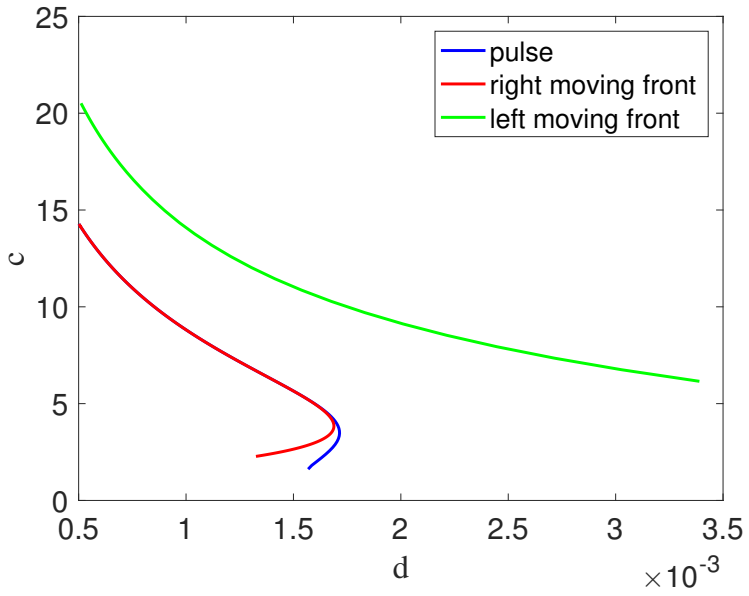

FIGURE 4.2.1: bifurcation curves for traveling pulses and fronts when changing d

For traveling fronts moving to the right, we perform the same procedures as for a traveling pulse. It is seen that in Figure 4.2.1 there is a turning point at $d = 1.69e-3$. For $d > 1.69e-3$, there is no traveling front moving to the right. It is also clear that when $d < 1.69e-3$ with d being close to a turning point, there are two traveling fronts moving to the right; the fast and the slow waves. Such a bifurcation diagram agrees with what we observe in the steepest descent method. Again we expect the

slow wave speed c_1 goes to 0 at some finite d, but finding this segment of bifurcation curve proves to be too difficult.

The bifurcation diagram for the left moving traveling front is represented in Figure 4.2.1. We see that there is no turning point. However when $d > 3.3898e-3$, our algorithm fails for large values of d because complex numbers start to appear in the calculations. This can be explained as follows. Linearization of the FitzHugh-Nagumo equations near $x = \infty$ leads to (3.3.1). The eigenvalue of the matrix A in the equation satisfies (3.3.2). As long as λ is real, both roots λ_1 and λ_2 are positive. With $\gamma = 8.6984$, $\beta = 0.25$, we see that λ is real as long as $d \notin (0.0037, 0.22)$. In such case the negative root s_2 of $s^2 + s - \frac{\lambda_1}{c^2} = 0$ is well defined. We can then impose the asymptotic boundary condition $u' \sim s_2 u$ and $v' \sim s_2 v$ at large x.

At the same time linearization of the front near $x = -\infty$ leads to (3.3.12). We can impose the asymptotic boundary condition there only when $d \notin (0.0031, 0.08)$. In such cases the negative root s_3 of $s^2 + s - \frac{\lambda_1}{c^2} = 0$ is well defined. We can then impose the asymptotic boundary condition $u' \sim s_3 u$ and $v' \sim s_3 v$ as $x \to -\infty$. It is observed that when $d > \min\{0.0037, 0.0032\} = 0.0031$, complex s_3 starts to appear. Hence the asymptotic boundary condition is incorrect. Though the algorithm yields solutions up to $d = 3.3898e-3$, the solution for $0.0031 < d < 3.3898e-3$ is not trust worthy.

4.2.2 Solution dependence on γ

Fix $\beta = 0.25$ and $d = 5.0e-4$ and allow γ to vary. To initiate the pseudo arc length continuation method, we use the fast traveling pulse solution (u, v, c) obtained from the steepest descent algorithm. The continuation algorithm yields a bifurcation

diagram whose projection on the (γ, c) plane is represented in Figures 4.2.2. When $7.1111 < \gamma < 10.2857$ (the constraint described by (1.1.1)), there is a traveling pulse. We find that traveling pulse continues to exist when $\gamma < 7.1111$. However if γ is slightly larger than 10.2857, no traveling pulse is found. In Figure 4.2.3 we compare the pulse profiles of u and v at various γ as it approaches 10.2857; it is seen that the width of the pulse increases rapidly. We speculate that such a width becomes infinitely long in the limit so that a pulse becomes a front. Numerical inaccuracy prevents us from determining the exact value of the transition γ.

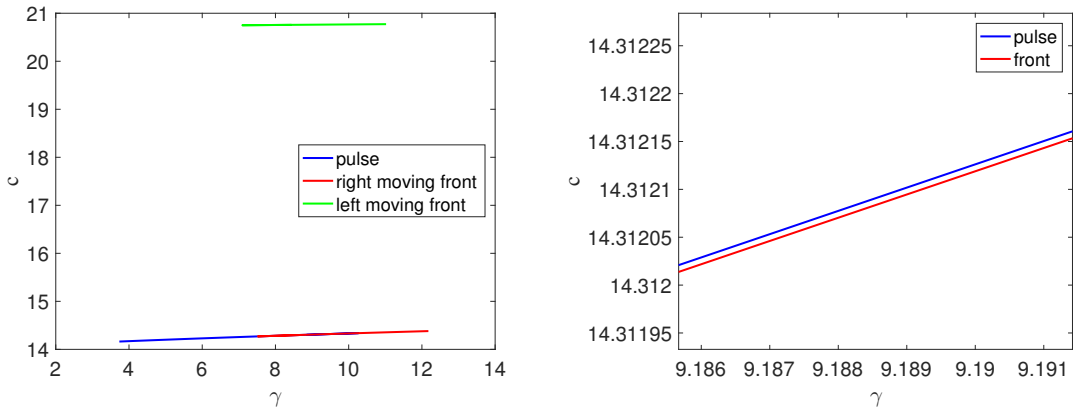

FIGURE 4.2.2: bifurcation curves for traveling pulses and fronts when changing γ

For traveling fronts moving to the right and the left, we perform the same procedures as for a traveling pulse. It is seen that in Figures 4.2.2 when $7.1111 < \gamma < 10.2857$, there are traveling fronts moving to the right and the left. Both types of traveling fronts continue to exist when $\gamma > 10.2857$. When $\gamma < 7.1111$, $(u, v) = (0, 0)$ is the only unique constant equilibrium solution. Hence it is no surprise that no traveling fronts are found for this range of γ. In fact numerical results find no traveling front at around $\gamma \cong 7.5286$. This can be explained as follows. When $\widetilde{\gamma}_1 = 7.5643$, the

line $v = \frac{u}{\widetilde{\gamma}_1}$ intersects the graph $v = f(u)$ at its local maximum point. For $\gamma_1 < \gamma < \widetilde{\gamma}_1$ it should be $f'(\mu_3) > 0$. The asymptotic boundary condition treatment in Section 3.3.3 breaks down, because the eigenvalue $\widehat{\lambda}_1$ may not be positive any more.

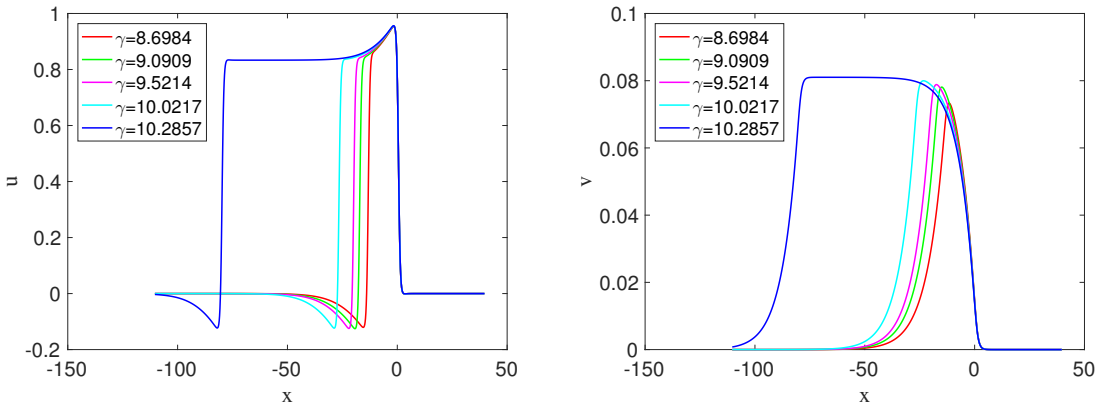

FIGURE 4.2.3: Compare fast wave profiles of u and v for pulse at different γ.

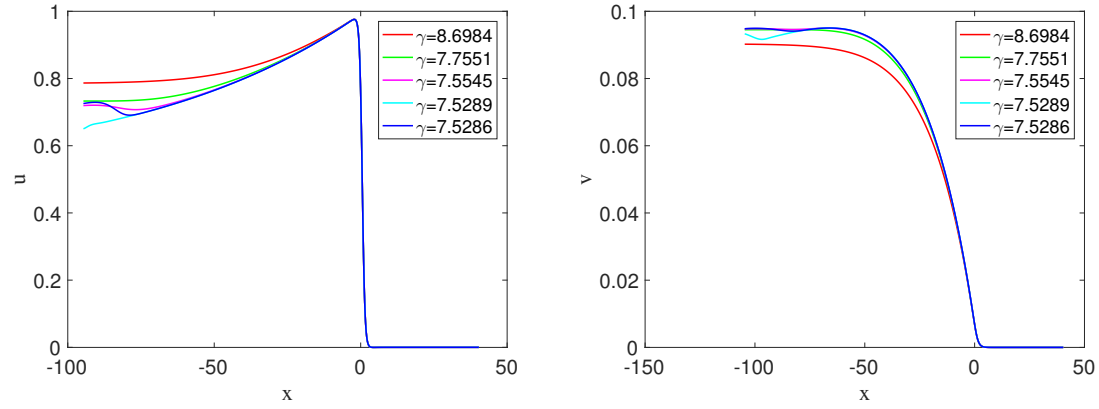

FIGURE 4.2.4: Compare fast wave profiles of u and v for front moving to the right at different γ.

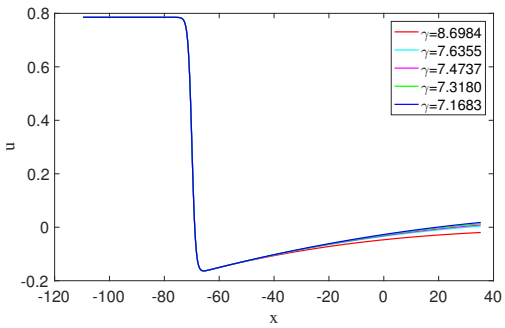

FIGURE 4.2.5: Compare profiles of u for front moving to the left at different γ.

Bibliography

[1] R. Burden, J. Faries, Numerical analysis. seventh edition, Brooks/cole (2001).

[2] C.-N. Chen, Y. S. Choi, Traveling pulse solutions to FitzHugh-Nagumo equations, Calc. Var. Partial Differential Equations 54 (1) (2015) 1-45.

[3] C.-N. Chen, Y. S. Choi, Standing pulse solutions to FitzHugh-Nagumo equations, Arch. Ration. Mech. Anal. 206 (3) (2012) 741-777.

[4] C.-N. Chen, Y. S. Choi, Front propagation in both directions and coexistence of distinct traveling waves, to be submitted.

[5] Y. S. Choi, J. M. Connors, A global algorithm for the computation of traveling pulses. Preprint.

[6] G. D. Smith Numerical Solution of Partial Differential Equations: Finite Difference Methods third Edition (1986).

[7] Y. S. Choi, P. J. McKenna, A mountain pass method for the numerical solution of semilinear elliptic problems, Nonlinear Anal. 20 (4) (1993) 417-437.

[8] P. C. Fife and J. B. Mcleod. The approach of solutions of nonlinear diffusion equations to traveling front solutions, Arch. Rational Mech. Anal. 65 (1977), 335-361.

[9] H.B. Keller, Lectures on Numerical Methods in Bifurcation Problems, Springer-Verlag, 1987.

[10] A.N. Kolmogorov, I.G. Petrovskii and N.S. Piskunov. Study of the diffusion equation with growth of the quantity of matter and its application to a biological problem. Bull. Univ. Moscow, Ser. Int. Sec. A 1 (1937).

[11] A. Volpert, V. Volpert and V. Volpert, Traveling Wave Solutions of Parabolic Systems. American Mathematical Society, Providence, 1994.

[12] D.G. Aronson and H.F. Weinberger. Multidimensional nonlinear diffusion arising in population genetics. Adv. in Math. 30 (1978), no. 1, 33-76.

[13] https://en.wikipedia.org/wiki/Reaction-diffusion system

[14] [FD] https://en.wikipedia.org/wiki/Finite-difference-wefficient